INTERACTIONS BETWEEN TWO REGULATORY PROTEINS OF MICROTUBULE DYNAMICS, HDAC6, TPPP/p25, AND THE HUB PROTEIN, DYNLL/LC8

Judit Oláh[a*], Sándor Szunyogh[a], Tibor Szénasi[a], Tamás Szaniszló[b], Adél Szabó[a], Attila Lehotzky[a], Tímea Berki[c], László Nyitray[d], Judit Ovádi[a*]

[a]Institute of Enzymology, Research Center for Natural Sciences, Hungarian Academy of Sciences, Budapest 1117, Hungary; [b]MTA-ELTE Lendület Bioinformatics Research Group, Eötvös Loránd University, Budapest 1117, Hungary; [c]Department of Immunology and Biotechnology, Medical School, University of Pécs, Pécs 7624, Hungary; [d]Department of Biochemistry, Eötvös Loránd University, Budapest 1117, Hungary.

*To whom correspondence should be addressed: Prof. Judit Ovádi and Judit Oláh, Institute of Enzymology, Research Center for Natural Sciences, Hungarian Academy of Sciences, Magyar tudósok körútja 2., H-1117 Budapest, Hungary; Telephone: +(36)1-3826-714; E-mail: ovadi.judit@ttk.mta.hu; olah.judit@ttk.mta.hu;

Judit Oláh: olah.judit@ttk.mta.hu; Sándor Szunyogh: szunyogh.sandor@ttk.mta.hu;
Tibor Szénási: szenasi.tibor@ttk.mta.hu; Tamás Szaniszló: tszaniszlo@caesar.elte.hu;
Adél Szabó: szabo.adel@ttk.mta.hu; Attila Lehotzky: lehotzky.attila@ttk.mta.hu;
Tímea Berki: berki.timea@pte.hu; László Nyitray: nyitray@elte.hu;
Judit Ovádi: ovadi.judit@ttk.mta.hu;

ABSTRACT

Degradation of unwanted proteins is important in protein quality control cooperating with the dynein/dynactin-mediated trafficking along the acetylated microtubule (MT) network. Proteins associated directly/indirectly with tubulin/MTs play crucial roles in both physiological and pathological processes. Our studies focus on the interrelationship of the tubulin deacetylase HDAC6, the MT-associated TPPP/p25 with its deacetylase inhibitory potency and the hub dynein light chain DYNLL/LC8, constituent of dynein and numerous other protein complexes. In this paper, evidence is provided for the direct interaction of DYNLL/LC8 with TPPP/p25 and HDAC6 and their assembly into binary/ternary complexes with functional potency. The in vitro binding data was obtained with recombinant proteins and used for mathematical modelling. These data and

visualization of their localizations by bimolecular fluorescence complementation technology and immunofluorescence microscopy in HeLa cells revealed the promoting effect of TPPP/p25 on the interaction of DYNLL/LC8 with both tubulin and HDAC6.Localization of the LC8-2-TPPP/p25 complex was observed on the MT network in contrast to the LC8-2-HDAC6 complex, which was partly translocated to the nucleus. LC8-2 did not influence directly the acetylation of the MT network. However, the binding of TPPP/p25 to a new binding site of DYNLL/LC8, outside the canonical binding groove, counteracted the TPPP/p25-derived hyperacetylation of the MT network. Our data suggest that multiple associations of the regulatory proteins of the MT network could ensure fine tuning in the regulation of the intracellular trafficking process either by the complexation of DYNLL/LC8 with new partners or indirectly by the modulation of the acetylation level of the MT network.

KEYWORDS

Tubulin Polymerization Promoting Protein/p25, DYNLL/LC8, histone deacetylase 6, ternary complexes, acetylation, intracellular trafficking

1. INTRODUCTION

The highly dynamic microtubule (MT) network, integral part of the eukaryotic cytoskeleton, plays crucial roles in cell division, differentiation, motility, intracellular trafficking and the maintenance of cell shape and polarization as well as in pathological conditions including inclusion body formation [1,2]. The dynamic instability [3], a characteristic behavior of MTs, is central to their functions that allows the rapid reorganization, differentiation spatially and temporally in accordance with environmental signals/factors. The stability and dynamics of MT network are regulated by post-translational modifications such as acetylation as well as by microtubule associated proteins (MAPs) [4-7]. Acetylation is regulated by the tubulin acetyltransferase αTAT1/MEC-17 [8,9] and atypical histone deacetylases such as histone deacetylase 6 (HDAC6). HDAC6 is ubiquitously expressed and localized primarily in the cytoplasm [10], and it is considered as the major tubulin deacetylase ([11] and references therein).

The brain-specific Tubulin Polymerization Promoting Protein (TPPP/p25) as a MAP regulates the dynamics and stability of the MT network via its tubulin polymerization promoting, MT bundling and tubulin acetylation enhancing activities [12-15]. The direct interaction of TPPP/p25 with HDAC6 results in the inhibition of the deacetylase activity of the enzyme, thus the

hyperacetylation of the tubulin/MT network [13,16]. TPPP/p25 is able to form dimers, which display enhanced tubulin polymerization promoting potency [17]. The disordered terminal segments of the protein, especially its C-terminus, are involved in the binding of TPPP/p25 to tubulin [18]; while the core region includes other binding segments such as an α-synuclein binding one [14,18]. The intracellular TPPP/p25 concentration is controlled by the ubiquitin-proteasome system; however, its over-expression mimics pathological conditions and produces specific ultrastructures such as aggresomes, which counteract the proteolytic degradation [19-21]. The aggresomes as membrane-less organelles are formed by the accumulation of small toxic amorphous aggregates and are degraded by the aggresome-autophagy pathway [22-25]. The failure of the clearing processes leads to the etiology of distinct human diseases, predominantly to neurological disorders. In fact, at pathological conditions, TPPP/p25 is co-localized and co-enriched with α-synuclein in Lewy bodies and glial cytoplasmic inclusions, characteristic for Parkinson's disease and multiple system atrophy, respectively; TPPP/p25 is a hallmark of synucleinopathies [26].

The two major degradation pathways responsible for the maintenance of the protein homeostasis within eukaryotic cells are the ubiquitin-proteasome system and the autophagy. The eventual clearance of the aggregates/aggresomes by the lysosome-dependent autophagic degradation is tightly coupled with the dynein-derived transport process ([27-29] and references therein). Malfunctioning of the components in this machinery including mutations in dynein subunits, loss of MT integrity, and inhibition or depletion of HDAC6 all lead to the failure of the trafficking pathway. HDAC6, in addition to its tubulin deacetylase activity, is also associated to MTs during the retrograde transport of the dynein motors and is intimately involved in aggresome formation as well as in the fusion of autophagosomes with lysosomes [30,31].

The large cytoplasmic dynein complex containing heavy, intermediate, light intermediate and light chains is the major molecular motor for retrograde movement of cargoes along the acetylated MT network [28,32]. Among the light chain subunits, the LC8 family members (DYNLL/LC8) are small (10 kDa) highly conserved ubiquitous eukaryotic homodimer proteins [33-35]. DYNLL/LC8 isoforms (LC8-1 and LC8-2) are essential components of the multi-subunit dynein complex; in addition, they are involved in multiple protein complexes of diverse systems [33,34,36,37]. Cellular studies showed that DYNLL/LC8 is associated to and transported along MTs together with its non-dynein partners [38]. This issue, however, has been questioned based upon the recognition that the dimeric DYNLL/LC8 by complexing the also dimeric dynein intermediate chain (DIC) is unable to bind simultaneously to cargo proteins as well [36,39]. Thus, DYNLL/LC8 has recently been defined as a hub protein [33,34,36,40].

In the studies presented here, we characterized the mutual interactions of these MT regulatory proteins, as well as their functional consequences related to the acetylation level of the MT network regulating both physiological and pathological processes.

2. MATERIALS AND METHODS

2.1. Plasmid constructs

Prokaryotic expression vector containing the insert for the human full length (FL) TPPP/p25 was prepared and purified as described previously [13,18]. The N-terminal truncated TPPP/p25 (NT, Δ3–43), the C-terminal truncated TPPP/p25 (CT, Δ175–219) and the double truncated TPPP/p25 (DT, Δ3–43/Δ175–219) were prepared as described previously [18] (Supplementary Fig. 1).

The sub-cloning plasmid pET21c–HDAC6 1-1215 was prepared to insert the full length HDAC6 cDNA into the pET21c, the following primers for polymerase chain reaction (PCR) amplification were used: 5′-GCTCACATATGACCTCAACCGGCCAGGATTCC-3′ (forward) and 5′-CCGCGGTCGACGTGTGGGTGGGGCATATCCTCCCC-3′ (reverse) and FLAG-tagged HDAC6 (a gift from Brian North, Harvard Medical School Boston, USA) as a template. The PCR product, after purification and digestion with NdeI-SalI restriction enzymes, was inserted to NdeI and XhoI sites in the pET21c vector (Novagen).The EGFP-HDAC6 was prepared by PCR using forward primer 5′-ATATGTCGACATATGACCTCAACCGGCCAGGATTCC-3′ and reverse primer 5′- GCAGCAGATCTTCAGTGGTGGTGGTGGTGGTGCTCG -3′ and pET21c–HDAC6 1-1215 as a template. The PCR product, following purification and after digestion with SalI-BglII restriction enzymes, was inserted to XhoI and BamHI sites in the pEGFP-C1 vector. The Halo-tagged HDAC6 construct was a gift from Cyril Barinka (Institute of Biotechnology CAS, Czech Republic) [41].

The coding sequence of LC8-2 was amplified and cloned in pmCherry-C1 vector using EcoRI and SalI restriction enzymes.

2.2. Bimolecular Fluorescence Complementation (BiFC) plasmids

The BiFC plasmids (pBiFC-V^{N1-173}, pBiFC-$V^{C155-238}$) were a gift of Prof. Péter Várnai (Semmelweis University, Budapest). The V^{N}-TPPP/p25 plasmid containing the insert for human FL TPPP/p25 was prepared as described previously [42]. Plasmid V^{C}-LC8-2 was produced by inserting the LC8-2 coding region in frame into pBiFC-$V^{C155-238}$ by EcoRI and SalI restriction enzymes. To insert the full length HDAC6 cDNA into the pBiFC-$V^{N1–173}$, the following primers

for PCR amplification were used: 5-ATATGTCGACATATGACCTCAACCGGCCAGGATTCC-3 (forward) and 5-GCAGCAGATCTTCAGTGGTGGTGGTGGTGGTGCTCG-3 (reverse) and pET21c–HDAC6 1-1215 as a template. The PCR product, following purification and after digestion with SalI-BglII restriction enzymes, was inserted to XhoI and BamHI sites in the BiFC vector. The sequences of all constructs were verified by restriction mapping and sequencing.

2.3. Expression and purification of human recombinant proteins

The C-terminal hexaHis fusion TPPP/p25 proteins were expressed in *E. coli* BL21 (DE3). The various TPPP/p25 truncated forms (Supplementary Fig. 1) were isolated on HIS-Select™ Cartridge (Sigma-Aldrich) as described previously [18].

LC8-1 and LC8-2 were prepared as described by [40]. Briefly, the ampicillin- and chloramphenicol-resistant cells were grown in Luria Bertani Broth containing 100 mg/l ampicillin, 30 μg/ml chloramphenicol and 1 mM $MgCl_2$ at 37 °C till 1.5-2 absorbance at 600 nm, then protein production was induced by the addition of 0.5 mM isopropyl β-D-1-thiogalactopyranoside. The cells were further incubated at 18 °C for 16 hours, then harvested by centrifugation (10 min, 4 °C, 5500 g). The pellet fraction was resuspended in phosphate buffer (10 mM Na_2HPO_4, 500 mM NaCl, pH 7.4 containing 5 mM imidazole, 0.5 mM phenylmethylsulfonyl fluoride, 5 mM benzamidine, 1 μg/ml pepstatin and 1 μg/ml leupeptin, 0.05 mg/ml lysozyme, 10 μg/ml DNAse and 50 μM tris(2-carboxyethyl)phosphine) and lysed by sonication. Following centrifugation (25 min, 4 °C, 39000 g), the supernatant containing the soluble proteins was affinity purified by Ni^{2+} affinity gel. The bound protein was eluted by 10 mM Na_2HPO_4, 500 mM NaCl, pH 7.4 containing 250 mM imidazole. After the affinity purification the buffer was changed to 20 mM tris(hydroxymethyl)aminomethane (Tris), 50 mM NaCl pH 8.0 by HiTrap desalting column (GE Healthcare) and the eluate was purified by anion exchange chromatography (buffer A: 20 mM Tris, 50 mM NaCl, buffer B: 20 mM Tris, 1 M NaCl). The protein containing fraction was further purified by gelfiltration chromatography (Superdex75 10/300 GL, GE Healthcare, buffer: 20 mM Tris pH 8.0, 150 mM NaCl). Then the proteins were concentrated and stored in 20 mM Tris, 150 mM NaCl pH 8.0, 10% glycerol and 1 mM dithioerythritol (DTE).

α-synuclein was prepared as described previously [43].

2.4. Tubulin preparation

Tubulin was prepared from bovine brain according to the method of Na and Timasheff [44].

2.5. *Determination of protein concentration*

Concentrations of the human recombinant proteins and tubulin were determined on the basis of the absorbance at 280 nm using the extinction coefficients evaluated by ExPASy-ProtParam tool (http://web.expasy.org/protparam): 10095 $M^{-1}*cm^{-1}$ for FL TPPP/p25, 10095 $M^{-1}*cm^{-1}$ for NT TPPP/p25, 5625 $M^{-1}*cm^{-1}$ for CT TPPP/p25, 5625 $M^{-1}*cm^{-1}$ for DT TPPP/p25, 15930 $M^{-1}*cm^{-1}$ for LC8-1, 14440 $M^{-1}*cm^{-1}$ for LC8-2, 5960 $M^{-1}*cm^{-1}$ for α-synuclein, 50310 $M^{-1}*cm^{-1}$ for tubulin, respectively.

The protein concentration of the cellular extracts was determined by the Bradford method [45].

2.6. *Affinity chromatography*

LC8-2 was immobilized to CNBr-activated Sepharose 4B (Amersham) according to the manufacturer's instructions. The LC8-2 bound to Sepharose was packed into columns. The binding capacity of a column was ~1.5 mg LC8-2 per 1 ml Sepharose (column volume ~ 2 ml). The affinity column was equilibrated with phosphate buffer (10 mM phosphate buffer pH 8.0 containing 10 mM NaCl). 0.25 mg TPPP/p25 or tubulin in 500 µl was loaded to the column, and the column was washed with phosphate buffer (5 ml, 0.5 ml fractions). The bound proteins were eluted with phosphate buffer containing 500 mM NaCl (5 ml, 0.5 ml fractions). After each experiment, the column was regenerated using 3 cycles of 0.1 M Na-acetate pH 4.0 buffer containing 0.5 M NaCl and 0.1 M Tris pH 8.0 buffer containing 0.5 M NaCl. Protein concentrations of the loaded, the unbound (wash) and the bound (eluted) fractions were determined on the basis of the absorbance at 280 nm. The unbound (wash) and the bound (eluted) fractions were analyzed by sodium dodecyl sulfate polyacrylamide gel electrophoresis (SDS-PAGE) as well.

2.7. *Enzyme-linked immunosorbent assay (ELISA) experiments*

ELISA assays were performed similarly as described previously [46]. Briefly, in the case of the DYNLL/LC8 isoforms, the plate was coated with 5 $\mu g \cdot mL^{-1}$ protein overnight in phosphate buffered saline (PBS), the wells were blocked with 1 mg/mL bovine serum albumin (BSA) in PBS for 1 h at room temperature. Then the partner proteins at a serial dilution (TPPP/p25 forms or tubulin or α-synuclein) or the various HeLa extracts at 1 mg/ml concentration were added. In another experimental set-up, the plate was coated with 5 $\mu g \cdot mL^{-1}$ tubulin or TPPP/p25 overnight in PBS, then LC8-2 at a serial dilution was added. The binding of the proteins of interest was

quantified by specific polyclonal TPPP/p25 [26] or monoclonal tubulin (Sigma T9026) or polyclonal HDAC6 (NB100-91805) or polyclonal α-synuclein (Sigma S3062) or polyclonal LC8-2 (16811-1-AP Proteintech) antibodies followed by addition of the secondary anti-rat (Sigma A9037) or anti-mouse (Sigma A2554) or anti-rabbit (TermoFisher Scientific 32260) IgG conjugated to horseradish peroxidase, respectively. The immunocomplex was quantified using o-phenylenediamine with hydrogen peroxide as substrate; absorbance was read at 490 nm with an EnSpire Multimode Reader (Perkin Elmer). Background value (no protein of interest is added to the plate) was subtracted in all cases. The apparent binding constants (K_d) were evaluated from the saturation curves by non-linear curve fitting assuming single binding site hyperbola model using the Origin 8.0 software.

In the case of the competitive ELISA experiments, LC8-2 was immobilized on the plate, tubulin at different concentrations was pre-incubated with 100 nM TPPP/p25 for 30 min at room temperature, then the binding of TPPP/p25 and tubulin to LC8-2 was detected by specific TPPP/p25 and tubulin antibodies, respectively, as described above. In another experimental set-up, the plate was coated with 2 $\mu g \cdot mL^{-1}$ HDAC6 (Merck Millipore 03-226), 500 nM LC8-2 was pre-incubated with 100 nM TPPP/p25 for 30 min at room temperature, then the binding of TPPP/p25 and LC8-2 was detected by specific TPPP/p25 and LC8-2 antibodies, respectively, as described above.

In the case of sandwich ELISA, the plate was coated with 1 μg/mL (50 μL/well) monoclonal TPPP/p25 antibody [47] in 200 mM Na_2CO_3 buffer pH 9.6 overnight at 4 °C. The wells were blocked with 1 mg/mL BSA in PBS for 1 h at room temperature. Next, the plate was incubated with 1 μM TPPP/p25 for 1 h at room temperature in PBS. Where indicated, TPPP/p25 was pre-incubated with 0.5 μM DYNLL/LC8, 2 μM DYNLL/LC8 or 10 μM Zn^{2+} or 100 μM DTE for 30 min at room temperature. Then the plate was sequentially incubated with biotinylated monoclonal TPPP/p25 antibody (1 μg/mL) [47] and peroxidase conjugated avidin (Calbiochem 189728) (2.5 μg/mL). Both antibodies were in PBS buffer containing 1 mg/mL BSA, and incubated for 1 h at room temperature. Between each incubation step, the wells were washed thrice with PBS containing 0.1% Tween 20 for 10 min. The presence of antibodies was detected using o-phenylenediamine as described above.

2.8. Mathematical modelling

All the numerical simulations were performed with Mathematica for Students (version 10.0.1.0) software package (Wolfram Research; http://www.wolfram.com). For the modelling, the

experimentally determined dissociation constants of the binary complexes were used. The binding affinities of the protein pairs within the ternary complex were varied to simulate the experimental data. The set of differential equations (see Supplementary data) was solved numerically, which allowed the determination of the complex formation and the concentrations characteristic for the equilibrium.

2.9. Circular dichroism (CD) spectroscopy

CD measurements were carried out on a Jasco J-720 spectropolarimeter at 20 nm/min scan rate, 8 s time constant and 1 nm step size in 10 mM phosphate buffer, pH 7.4 at room temperature. The path length was 0.1 cm. Protein concentrations were 4 μM for TPPP/p25, 1 μM for tubulin and 7 μM for LC8-2. The difference spectrum was obtained by subtracting the spectra of the individual proteins from that of the mixture of two proteins.

2.10. Fluorescence Polarization (FP)

FP experiments were carried out at 25 °C in Tris buffer (20 mM Tris, 100 mM NaCl, pH 7.4) supplied by 2 mM tris(2-carboxyethyl)phosphine and 0.05% Brij using a Synergy H4 (BioTek Instruments) plate reader. N-terminally Fluorescein 5-isothiocyanate (FITC) labeled, known binding peptide of DYNLL/LC8, BMF (TSQEDKATQTL) [40] was applied as an interacting partner of LC8 isoforms, and the influence of TPPP/p25 on this interaction was detected. Briefly, 50 nM labeled BMF peptide was mixed with LC8-1 or LC8-2 in a concentration to achieve 80% complex formation determined by direct titration (12 μM for LC8-1, and 8 μM for LC8-2, respectively). Subsequently, increasing amounts of FL or DT TPPP/p25 was mixed to the formed complexes and the change in polarization was measured.

2.11. Polymerization assay and pelleting experiments

The assembly of tubulin (6 μM) was performed in polymerization buffer (50 mM 2-(N-morpholino)ethanesulfonic acid buffer, pH 6.6, containing 100 mM KCl, 1 mM DTE, 1 mM $MgCl_2$, and 1 mM ethylene glycol tetraacetic acid) at 37 °C in the presence of TPPP/p25 (3 μM calculated for the monomeric form) with or without DYNLL/LC8 (10 or 20 μM calculated for the monomeric form). The tubulin polymerization was induced by the addition of TPPP/p25 or TPPP/p25 premixed with DYNLL/LC8. The optical density was monitored at 350 nm by a Cary 100 spectrophotometer (Varian, Walnut Creek, Australia).

In the pelleting experiments, TPPP/p25 (3 μM), DYNLL/LC8 (10 μM), tubulin (6 μM) or paclitaxel-assembled MTs (6 μM) and their various mixtures were incubated in polymerization

buffer at 37 °C for 15 min. When indicated, one or two of the proteins were preincubated (in polymerization buffer at 37 °C for 15 min) before added to the partner, then the final mixture was incubated in the same way. The samples (100 µl aliquot) were centrifuged (15 min, 37 °C, 17000 g), and the pellet (P) and the supernatant (S) fractions were separated. The pellet fractions were resuspended in 100 µl polymerization buffer. The fractions were analyzed by SDS-PAGE. MM indicates the molecular weight marker (PageRuler Prestained Protein Ladder, Thermo Scientific 26616).

2.12. Extract preparation from HeLa cells transfected with HDAC6

HeLa cells (ATCC® CCL-2™, American Type Culture Collection) were grown in Dulbecco's modified Eagle's medium supplemented with 10% fetal calf serum and 100 µg/ml kanamycin in a humidified incubator at 37 °C with 5% CO_2. Cells were grown on 60 mm Petri dishes and were transfected with 2 µg or 6 µg HDAC6 (Halo-tagged HDAC6) [41] using 12 µl Turbofect Transfection Reagent (Thermofisher), and incubated overnight. Control and transfected cells were collected on the next day, washed with medium, then with PBS three times, centrifuged (2 min, room temperature, 200 g) between the washing steps, then suspended in lysis buffer (50 mM Tris, 100 mM NaCl, pH 7.5 containing 0.5% NP-40). After centrifugation (10 min, 4 °C, 13,000 g), the supernatant was used for ELISA and HDAC6-activity assay. The protein concentration was determined by the Bradford method [45]. The extract of HDCA6-transfected HeLa cells were also electrotransferred onto Immobilon-PSQ transfer membranes and subjected to Western blot. The blot was developed using monoclonal tubulin (Sigma T9026) or polyclonal HDAC6 (NB100-91805) antibodies followed by addition of the secondary anti-mouse (Sigma A2554) or anti-rabbit (TermoFisher Scientific 32260) IgG conjugated to horseradish peroxidase, respectively. Peroxidase reaction was detected using Immobilon Western substrate (Millipore) by a Bio-Rad ChemiDoc MP Imaging system and its ImageLab 4.1 software.

2.13. HDAC6 activity assay by Western blot

The extract of HDCA6-transfected HeLa cells was incubated with 1 µM tubulin, 100 µM $ZnCl_2$, and 0.1 mg/ml BSA without or with 10 µM LC8-2 in assay buffer (BPS Bioscience, 50031) for 1 h at 37 °C. Trichostatin A (TSA) (1 µM), which is a HDAC6 inhibitor [48], was used as a positive control. The same samples were electrotransferred onto Immobilon-PSQ transfer membranes and subjected to Western blot. The blot was developed using a monoclonal mouse antibody against acetylated α-tubulin at Lys-40 (1:5000, clone 6-11B-1, Sigma T6793), antibody

binding was revealed by anti-mouse IgG-peroxidase conjugate (Fc-specific), (1:5000, Sigma A2554). Peroxidase reaction was detected using Immobilon Western substrate (Millipore) by a Bio-Rad ChemiDoc MP Imaging system and its ImageLab 4.1 software. Then amido black solution (0.1% w/v amido black, 25% v/v isopropanol and 10% v/v acetic acid) was applied for 1 min to stain the protein bands on the membrane. Intensity of bands was analyzed by ImageJ 1.49 using Measure command and subtracting background values.

2.14. Cell culture, manipulation and images

For the evaluation of the Venus signal, HeLa cells grown on 12-mm-diameter glass coverslips were transfected with the Venus fragments V^C-LC8-2 and V^N-TPPP/p25 or V^N-HDAC6, along with the full length TPPP/p25 or HDAC6 plasmids in the competition studies; in another experiment, mCherry-C1-LC8-2 [35] and EGFP-HDAC6 plasmids were transfected with Turbofect (Invitrogen) transfection reagent, according to the manufacturer's protocol.

After treatment, the cells were fixed with −20 °C methanol for 10 min, followed by postfixation with 4% formaldehyde (Sigma) for 2 min. After washes with PBS (3 × 10 min), samples were blocked for 30 min in PBS with 0.1% Triton X-100 (Sigma) containing 5% fetal calf serum.

Mouse monoclonal tubulin (Sigma T9026), mouse monoclonal acetyl-tubulin (Sigma T6793) and rat polyclonal TPPP/p25 [26] primary antibodies were used with Alexa 546 conjugated mouse (Thermo Fisher Scientific A11030), Alexa 488 conjugated mouse (Thermo Fisher Scientific A11029) or Alexa 546 conjugated rat (Thermo Fisher Scientific A11081) secondary antibodies. Nuclei were counterstained with 4′,6-diamidino-2-phenylindole (DAPI).

For the quantitative analysis of the images, the pictures were taken under constant exposure parameters. The determination of the BiFC and acetyl-tubulin signals were performed by using the Analyze, Measure option of the National Institutes of Health ImageJ software with the original grayscale pictures without modification. In each case, at least 40 cells were analyzed; whole territory of each cell was outlined by the Freehand Line tool and integrated pixel densities were calculated by multiplying the area of each cell with the corresponding average pixel intensity after subtracting the background.

Images of the mounted samples were acquired on a Leica DM IL 500 microscope equipped with Leica DFC 395 FX camera and HBO 100w lamp.

The equipment software was Leica Application Suite 4.4.0.; Chroma UV filter set (No. C40888), Chroma 41028 HQ NB GFP filter set (No. C21116), Chroma 41028 Y GFP filter set (No. C2117) and Leica filter N2.1 (No. 513832) was used for DAPI, EGFP, Alexa 488, BiFC and

Alexa 546 or mCherry signal acquisition, respectively, using a HCX FL Fluotar 40x/0.75 (dry) objective. RGB images were created using Adobe Photoshop CS2 by copying the original greyscale microscopic images (1600 × 1200 pixels, 600 dpi, 8-bit tiff images) into the corresponding red, green, or blue channel, respectively. A minimal background correction was applied by the same way for channels of the selected subpictures. In the presented images, original pixel density was changed to 300 dpi without recalculation.

2.15. Statistics

The error bars represent the standard deviation (SD). Comparisons were performed using the two-sided, unpaired Student's t-test and values were considered to be significant if the calculated p value was <0.05 (*).

3. RESULTS

3.1. Multiple interactions of LC8-2 with TPPP/p25 and tubulin

The unstructured, multifunctional protein, TPPP/p25 has been extensively characterized concerning its structural and functional features [4,14,42]. Distinct binding segments, its flexible CORE region and the extended unstructured termini were identified that are involved in multifarious interactions including its dimerization coupled with physiological function [4,14,42]. One of the light chains of the dynein complex, DYNLL/LC8, has recently been identified as a hub protein and it functions as a dimerization promoting effector [33]. This feature is originated from its symmetric homodimer structure with grooves at the dimer interface and its ability to bind to two identical short linear motifs, which are usually localized in the disordered segments of the targeted proteins. We hypothesized that the unstructured TPPP/p25 with its dimerization ability could be an interacting partner of DYNLL/LC8 that promotes its dimerization.

The interaction of LC8-2 with TPPP/p25 was tested by affinity chromatography. LC8-2 was immobilized onto CNBr-activated Sepharose 4B column as described in the Materials and Methods. TPPP/p25 or tubulin was loaded into the column, which retained the proteins according to its binding capacity. The flow-through (unbound) and the eluted (bound) fractions were analyzed by absorbance at 280 nm as well as by SDS-PAGE (Fig. 1A and Supplementary Fig. 2). As illustrated in Fig. 1A, TPPP/p25 binds to the immobilized LC8-2, it can be detected mainly in the bound fractions; while tubulin (loaded in comparable amount) partitions between the unbound and the bound fractions.

The interaction of TPPP/p25 with LC8-2 was quantified by ELISA experiments using human recombinant proteins. As shown in Fig. 1B, TPPP/p25 binds to the immobilized LC8-2 with a relatively high apparent affinity (K_d = 12.0 ± 3 nM), as evaluated by curve fitting. The binding affinity of TPPP/p25 to LC8-2 is comparable with that of TPPP/p25 and tubulin (K_d = 10.5 ± 1.2 nM) [49] or TPPP/p25 and HDAC6 (K_d = 5.3 ± 0.8 nM) [16]. Comparative binding studies carried out with the other isoform, LC8-1, underlined their similar binding capability to TPPP/p25 (Supplementary Fig. 3A).

Previously we reported the *neomorphic chameleon* character of TPPP/p25, namely that in spite of the deletion of its distinct segments, the protein can maintain its binding potency to α-synuclein [46]; this propensity was tested in relation to LC8-2. Various truncated forms of the human TPPP/p25 (Supplementary Fig. 1) were produced by recombinant techniques (cf. Materials and Methods) to perform ELISA experiments similarly as with the FL TPPP/p25. As illustrated in Fig. 1B, the truncations of TPPP/p25 do not cause significant differences in their interaction with LC8-2, each truncated TPPP/p25 form does bind LC8-2 due to its high conformational plasticity. However, it needs to be noted that no binding of α-synuclein, a non-MT protein, to LC8-2 was detected in a control ELISA experiment (Fig. 1B).

To characterize the interaction of LC8-2 with tubulin and to evaluate the possible effect of TPPP/p25 on this interaction, the following sets of ELISA experiments were performed (Fig. 1C and 1D). LC8-2 was immobilized on the plate, and then tubulin was added at various concentrations pre-incubated without and with constant TPPP/p25. The binding of TPPP/p25 or tubulin to the immobilized LC8-2 was determined by specific antibodies as described in the Materials and Methods. These experimental set-ups allowed the quantitative detection of the potential complex formation by immunostaining. The ELISA experiments underline the observation obtained with affinity chromatography, namely, the interaction of LC8-2 with tubulin is much weaker than that with TPPP/p25. As shown in Fig. 1D, the amount of TPPP/p25 associated to LC8-2 decreased by increasing the tubulin concentration, which may indicate a competition of tubulin and LC8-2 for TPPP/p25 binding. However, in a similar set of experiment, TPPP/p25 enhanced the binding of tubulin to the immobilized LC8-2 (Fig. 1C). This finding shows that both binary and ternary complexes of LC8-2 with TPPP/p25 and/or tubulin can be formed.

In order to reveal the nature of the binding properties of the complexes, an experiment-based mathematical model was developed that allows one to obtain quantitative data for the interactions forming simultaneously binary and ternary complexes. Two models were evaluated: a competitive model assuming exclusively binary complexes and a ternary complex model allowing the

formation of the LC8-2-TPPP/p25-tubulin complex. The models include the experimentally determined apparent dissociation constants of the binary complexes (for details see Supplementary data and Supplementary Table S1). Fig. 1C and 1D show the binding of tubulin and TPPP/p25 to the immobilized LC8-2 as well as the theoretical curves. The coincidence of the experimental and computed curves supports the formation of binary and ternary complexes, the ratios of which are determined by the concentrations of the partner proteins that could produce apparent competition.

3.2. Structural consequences of the interaction of TPPP/p25 and LC8-2

The effect of the binding of LC8-2 to TPPP/p25 on the secondary structure of the disordered TPPP/p25 was detected by CD spectroscopy. Both LC8-2 and tubulin display CD spectra corresponding to globular proteins (Fig. 2A and B), while the spectrum of TPPP/p25 with a minimum at 205 nm is characteristic for disordered proteins [12]. Previously we provided evidence that the interaction of tubulin and TPPP/p25 resulted in secondary structural alteration likely in the disordered TPPP/p25 as reflected by a difference ellipticity spectrum with a maximum at nearly 207 nm [12] (Fig. 2A). The interaction of LC8-2 and TPPP/p25 generated a similar, but much smaller spectral alteration (Fig. 2B) as that of tubulin and TPPP/p25, in spite of the fact that they display similar binding affinities to TPPP/p25 (cf. Fig. 1).

LC8-2 has been proposed to function as a “dimerization engine” promoting the association of partner proteins [33]. TPPP/p25 occurs both in monomeric and dimeric forms, further stabilized by inter-chain disulfide bridges; the dimeric TPPP/p25 displays enhanced tubulin polymerization promoting potency indicating that the dimer may be the physiologically relevant form [17]. Therefore, we investigated the effect of LC8-2 on the dimerization of TPPP/p25 by sandwich ELISA. This is a suitable method to detect dimer/oligomer forms using a monoclonal antibody and its biotinylated form [50]. In this case, monoclonal TPPP/p25 antibody [47] was immobilized on the plate, and TPPP/p25 pre-incubated with or without LC8-2 was added to the plate, then the same monoclonal TPPP/p25 antibody in its biotinylated form was added, the binding of which was detected through peroxidase conjugated avidin reaction. This ELISA assay allows the detection of the dimeric/oligomeric TPPP/p25, since monomers cannot bind simultaneously to the immobilized and the biotinylated antibodies with the same epitope [21]. As shown in Fig. 2C, the amount of dimeric TPPP/p25 detected in the control is slightly reduced in the presence of LC8-2; and it is further reduced in the presence of DTE, a disulfide reducing agent. As a positive control, zinc cation was added to TPPP/p25, which is known to promote its dimerization [21]. According to the expectation, the amount of the dimeric TPPP/p25 form significantly increased. These findings indicate that the binding of LC8-2 to TPPP/p25 does not promote the dimerization of

TPPP/p25. Similar results were obtained in experiments carried out with the other isoform, LC8-1 (Supplementary Fig. 3B).

To further investigate this unexpected behavior, FP measurements were carried out. LC8-2 was incubated with the FITC-labeled BMF peptide, a known LC8-2 ligand that binds to the identical parallel grooves of the dimeric LC8-2 [34,40]. Control experiments have shown that the direct binding of the FITC-BMF peptide to DYNLL/LC8 isoforms in the FP assay resulted in K_d values corresponding to the published ones [40] (Supplementary Fig. 3C). Then TPPP/p25 was added to LC8-2 complexed with the FITC-BMF peptide (Fig. 2D and Supplementary Fig. 3D), and its effect on the FP of the peptide-associated LC8-2 was determined. Assuming competition of TPPP/p25 and the FITC-labeled BMF peptide for the binding of LC8-2, the release of the peptide from the groove of LC8-2 resulting in reduced FP can be expected. However, no release of the peptide was detected; on the contrary, FP signal increased as a function of TPPP/p25 concentration. Similar observation was made when DT TPPP/p25 was added instead of FL TPPP/p25 protein or LC8-1 isoform was applied instead of LC8-2 (Supplementary Fig. 3D). As a positive control, the DIC peptide was used [34,51], and competition was detected as described earlier. These findings strongly suggest that TPPP/p25 does bind to LC8-2, but not to the well-established binding grooves available for the consensus LC8-2 binding peptides. Furthermore, these results provide an explanation for the failure of the LC8-2-promoted dimerization of TPPP/p25 (cf. Fig. 2C). Therefore, these data suggest the existence of a new "exosite" binding domain on LC8-2, likely the α-helices flanking the β-sheet dimerization interface. This issue is in agreement with the fact that no potential consensus LC8-2 binding motif [52] in TPPP/p25 could be identified.

3.3. Effect of LC8-2 on the TPPP/p25-derived tubulin assembly

The unstructured TPPP/p25 as a MAP regulates the dynamics and stability of the MT network via its tubulin polymerization promoting and MT bundling activities [14]. The effect of LC8-2 on these functions of TPPP/p25 was studied by two sets of experiments: i) TPPP/p25-induced tubulin polymerization as detected by turbidimetry; and ii) the partition of the polymerized forms of the proteins in a pull-down experiment.

Fig. 3A shows an unusual tubulin polymerization curve that, however, is typical for the TPPP/p25-promoted tubulin polymerization coupled with MT bundling and the formation of aberrant MT species as demonstrated earlier by electron microscopy [12,53] (Fig. 3B). The characteristic assembly of tubulin by TPPP/p25 as followed by turbidimetry was not affected significantly by either LC8-2 or LC8-1 (Fig. 3A and Supplementary Fig. 4A). Next, the effect of

LC8-2 on the partition of the monomeric and assembled tubulins induced by TPPP/p25 was studied in pelleting experiments. Tubulin (Fig. 3C) or paclitaxel-assembled MTs (Fig. 3D) were incubated with human recombinant TPPP/p25 and/or LC8-2. The samples were pelleted and analyzed by SDS-PAGE that allowed us the quantification of the partition of soluble and assembled forms. Fig. 3C and 3D show the partition of the proteins in the supernatant and pellet fractions. TPPP/p25 can be detected mainly in the pellet fraction, when it was incubated with tubulin/MTs, in agreement with our previous results [15,18]. Significant amount of LC8-2 could also be detected in the pellet only in the presence of TPPP/p25 (when all three proteins were present), indicating a crucial role of TPPP/p25 in promoting the binding of LC8-2 to the tubulin-containing fractions. LC8-1 isoform behaved similarly (Supplementary Fig. 4B and C). However, it is not clear whether the binding sites are distinct for the partner proteins or TPPP/p25 induces a piggy-back binding within the ternary complex.

3.4. HDAC6 is a new interacting partner of LC8-2

Previously we reported the inhibitory effect of TPPP/p25 on HDAC6, a tubulin deacetylase enzyme, caused by their mutual interaction leading to the elevation of the acetylation level of the MT network [13]. The maintenance of the acetylation level of the MT network is a crucial issue in the dynein-derived trafficking process, in which HDAC6 plays an important role as a scaffold protein [31,32,54,55]. Since our previous studies have shown the association of HDAC6 with TPPP/p25 resulting in decreased deacetylase activity/increased tubulin acetylation, we decided to evaluate the influence of LC8-2 on tubulin acetylation by performing both binding and functional studies.

HeLa cells were transfected with HDAC6 and the intracellular level of HDAC6 in the extracts depending on the transfection (2 or 6 μg plasmid) was determined by Western blot (Fig. 4A and Supplementary Fig. 5). In an ELISA experiment, LC8-2 was immobilized onto the plate, and the binding of HDAC6 was quantified using a specific antibody as described in the Materials and Methods (Fig. 4B). As illustrated in Fig. 4B, HDAC6 from the cell extract did bind to the immobilized LC8-2. In another set of experiments, TPPP/p25, LC8-2 or their preincubated mixture were added to the immobilized HDAC6, and the binding of proteins to HDAC6 was detected by specific antibodies as described in the Materials and Methods. As shown in Fig. 4C, LC8-2 slightly decreased the binding of TPPP/p25 to HDAC6, however, TPPP/p25 significantly increased the association of LC8-2 to the tubulin deacetylase enzyme immobilized onto the plate. This finding suggest that besides binary complexes, ternary complex of TPPP/p25, HDAC6 and LC8-2 are formed as well.

As we reported earlier, the MT network in HeLa cells is practically deacetylated; however, HDAC6 inhibitors such as TSA or TPPP/p25 promote the hyperacetylation of the MT network [13,16]. Functional assays have been established to study the effect of LC8-2 on the HDAC6-mediated tubulin acetylation using isolated acetylated tubulin as a substrate. As shown in Fig. 5A and Supplementary Fig. 6, no acetylated tubulin can be detected in the transfected HeLa extracts. However, the addition of HeLa extract transfected with HDAC6 reduced the acetylation level of the isolated tubulin. The addition of LC8-2 did not affect significantly the acetylation level of tubulin, a substrate of HDAC6. TSA was used as a well-established HDAC6 inhibitor, which indeed suspended HDAC6 activity. These data have revealed that the direct association of LC8-2 to HDAC6 does not affect the activity of the deacetylase enzyme significantly.

However, LC8-2 may exert indirect effect on the acetylation level of the MT network through its interaction with TPPP/p25. This question was investigated in HeLa cells transfected with LC8-2, TPPP/p25 or both proteins (Fig. 5B). As expected, TPPP/p25 promoted MT acetylation, while LC8-2 did not altered it significantly. As illustrated in Fig. 5B, the acetylation level of the MT network of HeLa cells co-transfected with LC8-2 and TPPP/p25 proteins was higher as compared to control cells, but lower than in cells transfected with TPPP/p25 alone. This observation indicates that although LC8 itself does not affect tubulin acetylation, it decreases the deacetylase inhibitory potency of TPPP/p25 within their ternary complex.

3.5. Interactions of LC8-2 in living cells

In order to validate the *in vitro* data at cellular level, immunofluorescence microscopy coupled with BiFC assays were applied for the visualization of the direct association of LC8-2 with TPPP/p25 and HDAC6 in living HeLa cells. The same method was used previously for the visualization of the intracellular binding of TPPP/p25 to sirtuin-2 and α-synuclein [15,46]. Venus fusion constructs of LC8-2 and TPPP/p25 as well as that of LC8-2 and HDAC6 were produced by recombinant technology, and the heteroassociations were visualized by fluorescence microscopy. As shown in the scheme (Fig. 6A), the N-terminal and the C-terminal segments of the fluorescent protein (Venus) were fused separately to HDAC6 and TPPP/p25 or LC8-2, respectively. The intracellular interaction of the labeled proteins brings the two segments of the split fluorescent protein in close proximity resulting in a BiFC signal, a fluorescence emission upon excitation.

First, the intracellular localizations of mCherry-labeled LC8-2 and EGFP-labeled HDAC6 were monitored in living HeLa cells by fluorescence microscopy as shown in Fig. 6B. While HDAC6 is localized mainly in the cytosol, LC8-2 is abundant also in the nucleus (Fig. 6B). By the application of BiFC technology, we provided evidence for the hetero-association of LC8-2-

HDAC6, occurring predominantly in the nucleus (Fig 6C). In fact, the interactions of HDAC6 with nuclear proteins (such as sumoylated p300, the transcriptional corepressor LCoR and transcription factors such as NF-κB and Runx2) have already been reported suggesting that HDAC6 may be involved in the regulation of transcription as well [56].

In another set of experiment, the intracellular interaction of LC8-2 and TPPP/p25 was tested by BiFC technology in living HeLa cells. The coupling of the Venus pairs indicates that LC8-2 interacts with TPPP/p25. In this set of BiFC experiments, the MT network was also stained (red). The BiFC complex of LC8-2 and TPPP/p25, in contrast to the LC8-2-HDAC6, was aligned along the MT network (Fig. 6C).

Control experiments revealed that neither the empty Venus vectors [42] nor the Venus fusion constructs of LC8-2 and α-synuclein produce a BiFC signal (Supplementary Fig. 7A), that concerns with the *in vitro* ELISA data (cf. Fig. 1B). To test the specificity of the BiFC signal, the cells were co-transfected with either unlabeled TPPP/p25 or HDAC6 as competitors of the corresponding Venus labeled partner proteins. As expected, co-transfection with the unlabeled TPPP/p25 or HDAC6 resulted in significant decrease of the intensity of BiFC complexes (Fig. 6D).

To assess their intracellular co-localization, the immunopositivity of TPPP/p25 (red) and the BiFC signal of the LC8-2-HDAC6 complex (green), were monitored (Fig. 6E). TPPP/p25 seemed to be aligned along the MT network in the transfected HeLa cells as we reported previously [19], while the LC8-2-HDAC6 complex (green) distributed both in the cytosol and the nucleus. To further examine the nature of their co-localization as well as to affirm the nuclear localization of the LC8-2-HDAC6 complex, line scans across the areas of interest in the transfected HeLa cell were generated and positivity of BiFC signal (green) and TPPP/p25 staining (red) were visualized by confocal microscopy (Supplementary Fig. 7B). In the transfected cells, there are areas with co-localization of TPPP/p25 and LC8-2-HDAC6 exclusively in the cytosol, while no TPPP/p25 but LC8-2-HDAC6 complex (green) can be visualized within the nucleus.

4. DISCUSSION

The DYNLL/LC8 dynein light chain isoforms are highly conserved ubiquitous eukaryotic proteins that were discovered as essential components of the MT-based molecular motor dynein involved in the retrograde intracellular trafficking [34]. More recently, evidence has been accumulated that DYNLL/LC8 isoforms also interact with proteins that are not connected with dynein or the MT-based transport, which introduced the idea that "its function as a dynein light

chain is but one of many" ([36] and references therein). In fact, DYNLL/LC8 is recognized as a regulatory hub protein; it is unlikely to bind cargo in the dynein complex, but is mainly involved in the dimerization of its partners [34].

However, the *Drosophila* LC8 homolog (94% identity with mammalian proteins), called Cut up, specifies the axonal transport of proteasomes; it binds proteasomes and functions specifically during their transport supporting a unique model for the dynein-mediated transport of neuronal proteasomes [57]. In addition, TPPP/p25 over-expression mimics pathological conditions and promotes aggresome formation [19,26], thus its assembly with DYNLL/LC8 and HDAC6 could be involved in the intracellular trafficking and/or aggresome-autophagy pathway (Fig. 7 and 8).

In this work, we identified two novel interacting partners of human DYNLL/LC8 paralogs (LC8-1 and LC8-2), HDAC6 and TPPP/p25, which are regulatory proteins of MT dynamics displaying different structural and functional characteristics [13,16] (Fig. 7). TPPP/p25 and HDAC6 mutually interact forming a functional complex resulting in the hyperacetylation of the MT network due to the inhibition of the tubulin deacetylase by TPPP/p25; and thus it has high impact on the trafficking processes [30]. HDAC6 specifically functions as an interlinker for the large dynein complex on the MT structure (Fig. 7B), however, the importance of its tubulin deacetylase activity in this process has been questioned [31].

Previously, when tight binding of any partners to the dimeric hub DYNLL/LC8 protein has been described, it resulted in the dimerization of the partner, mostly disordered proteins. This was not the case with TPPP/p25. Therefore, we hypothesize that the association of the DYNLL/LC8 hub proteins with TPPP/p25 is a consequence of their multivalent interactions with the unstructured TPPP/p25 similarly that has been reported in the case of its interaction with α-synuclein [46]. Interestingly, recently has been reported that DYNLL/LC8, which interacts with Bim and Bmf proteins and induces their homo-dimerization, may form a ternary Bim-DYNLL/LC8-Bmf complex as well [58].

We have identified a short linear peptide segment, $[D/S]_{-4}K_{-3}X_{-2}[T/V/I]_{-1}Q_0[T/V]_1[D/E]_2$, as a binding motif for most interacting partners of the hub DYNLL/LC8. These segments are usually localized in disordered segments of the DYNLL/LC8 binding proteins [33]. TPPP/p25 does not have a segment displaying significant homology with the canonical DYNLL/LC8 binding sequences [52,59]. In addition, no dimerization-promoting potency of DYNLL/LC8 could be detected in the case of the disordered TPPP/p25, in spite of the fact that it exists in a concentration-dependent monomer-dimer/oligomer equilibrium [17]. All these findings seem to underline that the nature of the association of TPPP/p25 and DYNLL/LC8 differs from that of other partners of the hub DYNLL/LC8 protein characterized by their binding to the parallel

grooves at the interface of the dimeric DYNLL/LC8 [34]. An alternative interaction surface (an "exosite") may exist on the outer surface of the dimeric protein. Indeed, in a docking model of DYNLL/LC8 bound to MTs, that surface interacts with tubulin [60]. Moreover, this outer surface contains "targeting specificity determining" residues [61], again suggesting that this surface might be involved in so far undescribed interaction site(s).

In contrast to the LC8-2-TPPP/p25 complex, the complex of LC8-2 with HDAC6 is partly translocated into the nucleus of HeLa cells (cf. Fig. 6). It could be an important issue since the potency of DYNLL/LC8 to promote/prevent translocation of various partners (Ciz1, METT-10, ATMIN) has been reported [35,62,63]. HDAC6 can be found mainly in the cytoplasm but it has been observed also in the nucleus [64]. Similar diffuse distribution of DYNLL/LC8 both in the cytoplasm and in the nucleus has been established, however, syntaphilin recruited DYNLL/LC8 to MTs resulting in their co-localization [65].

In conclusion, LC8-2 does not influence the acetylation of the MT network directly, however, the binding of LC8-2 to TPPP/p25 reduced the inhibitory potency of TPPP/p25 on HDAC6 counteracting the TPPP/p25-derived hyperacetylation of the MT network. On one hand, TPPP/p25 promotes the association of LC8-2 to the MT network that could be related to the dynamics/stabilization of the MT network. On the other hand, the association of LC8-2 to HDAC6, a newly discovered heteroassociation, is promoted by TPPP/p25 suggesting the formation of a ternary complex. The formation of the binary and ternary HDAC6 complexes could have epigenetic function by modulating the intracellular localization of HDAC6, a key histone deacetylase enzyme. The multiple interactions of the MT-related proteins, TPPP/p25, HDAC6 and LC8-2, may display a role in the fine-tuning of the dynein-derived trafficking process concerning the acetylation level of the MT network as well as the efficacy of the dynein-derived trafficking process (cf. Fig. 8).

5. LIST OF ABBREVIATIONS

Bimolecular fluorescence complementation (BiFC); bovine serum albumin (BSA); circular dichroism (CD); C-terminal truncated Tubulin Polymerization Promoting Protein (CT TPPP/p25); 4′,6-diamidino-2-phenylindole (DAPI); dithioerythritol (DTE); double truncated Tubulin Polymerization Promoting Protein (DT TPPP/p25); dynein intermediate chain (DIC); enzyme-linked immunosorbent assay (ELISA); fluorescence polarization (FP); fluorescein 5-isothiocyanate (FITC); full length Tubulin Polymerization Promoting Protein (FL TPPP/p25); histone deacetylase 6 (HDAC6); LC8 family member of dynein light chains (DYNLL/LC8); LC8

isoform 1 (LC8-1); LC8 isoform 2 (LC8-2); microtubule (MT); microtubule associated protein (MAP); N-terminal truncated Tubulin Polymerization Promoting Protein (NT TPPP/p25); phosphate buffered saline (PBS); polymerase chain reaction (PCR); sodium dodecyl sulfate polyacrylamide gel electrophoresis (SDS-PAGE); Trichostatin A (TSA); tris(hydroxymethyl)aminomethane (Tris); Tubulin Polymerization Promoting Protein (TPPP/p25).

6. COMPETING INTEREST

The authors declare that they have no competing interests.

7. FUNDING

This work was supported by the European Concerted Research Action COST Action [TD1406] and the Hungarian National Research, Development and Innovation Office Grants OTKA [T-112144, K-119359, and PD-124061] to J. Ovádi, L. Nyitray, and T. Szénási, respectively. T. Szaniszló thanks the support of the "Lendület" program from the Hungarian Academy of Sciences [LP2014-18] to Dr. Zs. Dosztányi. One of the authors (A. Szabó) thanks the József Varga Foundation for a Fellowship. The funders had no role in study design, data collection and analysis, decision to publish, or preparation of the manuscript.

8. AUTHORS' CONTRIBUTIONS

Judit Oláh: performing and supervising in vitro experiments, data collection and evaluations, responsibility for the research activity including mentorship to PhD fellows, manuscript preparation; Sándor Szunyogh: immunocytochemistry with HeLa cells, BiFC experiments; Tibor Szénási: production of constructs of the TPPP/p25 variants, cloning, expression of proteins, mVenus constructs for the BiFC technology; Tamás Szaniszló: purification of DYNLL/LC8, fluorescence polarization experiments; Adél Szabó: expression and isolation of the recombinant TPPP/p25 proteins, performing CD, pelleting and ELISA experiments, data collection and evaluation; Attila Lehotzky: planning and implementation of the HeLa cell experiments, cell manipulations, immunocytochemistry, fluorescence microscopy including mentorship to the PhD fellows; Tímea Berki: production of the monoclonal TPPP/p25 antibodies including the labeled ones for the sandwich ELISA experiments; László Nyitray: expert of DYNLL/LC8 biochemistry, interpretation of the in vitro data; Judit Ovádi: ideas, evolution and coordination of the research

aims, planning and execution, acquisition of the financial support for the in vitro and cellular studies, and manuscript preparation.

9. ACKNOWLEDGEMENT

We are grateful to Prof. Péter Várnai of the Physiology Department, Faculty of Medicine, Semmelweis University, Budapest, Hungary, for providing the mVenus BiFC plasmids and to Prof. Cyril Barinka, Institute of Biotechnology CAS, BIOCEV, Vestec, Czech Republic, for providing the Halo-HDAC6 plasmid.

10. REFERENCES

1. Conde C, Cáceres A. MT assembly, organization and dynamics in axons and dendrites. Nat Rev Neurosci. 2009;10(5):319-32.
2. de Forges H, Bouissou A, Perez F. Interplay between MT dynamics and intracellular organization. Int J Biochem Cell Biol. 2012;44(2):266-74.
3. Mitchison T, Kirschner M. Dynamic instability of MT growth. Nature. 1984 Nov 15-21;312(5991):237-42.
4. Oláh J, Tőkési N, Lehotzky A, Orosz F, Ovádi J. Moonlighting MT-associated proteins: regulatory functions by day and pathological functions at night. Cytoskeleton (Hoboken). 2013;70(11):677-85.
5. Ilan Y. MTs: From understanding their dynamics to using them as potential therapeutic targets. J Cell Physiol. 2019;234(6):7923-7937.
6. Konno A, Setou M, Ikegami K. Ciliary and flagellar structure and function--their regulations by posttranslational modifications of axonemal tubulin. Int Rev Cell Mol Biol. 2012;294:133-70.
7. Akhmanova A, Steinmetz MO. Control of MT organization and dynamics: two ends in the limelight. Nat Rev Mol Cell Biol. 2015;16(12):711-26.
8. Akella JS, Wloga D, Kim J, Starostina NG, Lyons-Abbott S, Morrissette NS, Dougan ST, Kipreos ET, Gaertig J. MEC-17 is an alpha-tubulin acetyltransferase. Nature. 2010;467(7312):218-22.
9. Shida T, Cueva JG, Xu Z, Goodman MB, Nachury MV. The major alpha-tubulin K40 acetyltransferase alphaTAT1 promotes rapid ciliogenesis and efficient mechanosensation. Proc Natl Acad Sci U S A. 2010;107(50):21517-22.

10. Hubbert C, Guardiola A, Shao R, Kawaguchi Y, Ito A, Nixon A, Yoshida M, Wang XF, Yao TP. HDAC6 is a MT-associated deacetylase. Nature. 2002;417(6887):455-8.
11. Li L, Yang XJ. Tubulin acetylation: responsible enzymes, biological functions and human diseases. Cell Mol Life Sci. 2015;72(22):4237-55.
12. Hlavanda E, Kovács J, Oláh J, Orosz F, Medzihradszky KF, Ovádi J. Brain-specific p25 protein binds to tubulin and MTs and induces aberrant MT assemblies at substoichiometric concentrations. Biochemistry. 2002;41(27):8657-64.
13. Tőkési N, Lehotzky A, Horváth I, Szabó B, Oláh J, Lau P, Ovádi J. TPPP/p25 promotes tubulin acetylation by inhibiting histone deacetylase 6. J Biol Chem. 2010;285(23):17896-906.
14. Oláh J, Bertrand P, Ovádi J. Role of the MT-associated TPPP/p25 in Parkinson's and related diseases and its therapeutic potential. Expert Rev Proteomics. 2017;14(4):301-309.
15. Szabó A, Oláh J, Szunyogh S, Lehotzky A, Szénási T, Csaplár M, Schiedel M, Lőw P, Jung M, Ovádi J. Modulation Of MT Acetylation By The Interplay Of TPPP/p25, SIRT2 And New Anticancer Agents With Anti-SIRT2 Potency. Sci Rep. 2017;7(1):17070.
16. Mangas-Sanjuan V, Oláh J, Gonzalez-Alvarez I, Lehotzky A, Tőkési N, Bermejo M, Ovádi J. Tubulin acetylation promoting potency and absorption efficacy of deacetylase inhibitors. Br J Pharmacol. 2015;172(3):829-40.
17. Oláh J, Zotter Á, Hlavanda E, Szunyogh S, Orosz F, Szigeti K, Fidy J, Ovádi J. MT assembly-derived by dimerization of TPPP/p25. Evaluation of thermodynamic parameters for multiple equilibrium system from ITC data. Biochim Biophys Acta. 2012;1820(7):785-94.
18. Tőkési N, Oláh J, Hlavanda E, Szunyogh S, Szabó A, Babos F, Magyar A, Lehotzky A, Vass E, Ovádi J. Identification of motives mediating alternative functions of the neomorphic moonlighting TPPP/p25. Biochim Biophys Acta. 2014;1842(4):547-57.
19. Lehotzky A, Tirián L, Tőkési N, Lénárt P, Szabó B, Kovács J, Ovádi J. Dynamic targeting of MTs by TPPP/p25 affects cell survival. J Cell Sci. 2004;117(Pt 25):6249-59.
20. Lehotzky A, Lau P, Tőkési N, Muja N, Hudson LD, Ovádi J. Tubulin polymerization-promoting protein (TPPP/p25) is critical for oligodendrocyte differentiation. Glia. 2010;58(2):157-68.
21. Lehotzky A, Oláh J, Szunyogh S, Szabó A, Berki T, Ovádi J. Zinc-induced structural changes of the disordered tppp/p25 inhibits its degradation by the proteasome. Biochim Biophys Acta. 2015;1852(1):83-91.

22. Lilienbaum A. Relationship between the proteasomal system and autophagy. Int J Biochem Mol Biol. 2013;4(1):1-26.
23. Nam T, Han JH, Devkota S, Lee HW. Emerging Paradigm of Crosstalk between Autophagy and the Ubiquitin-Proteasome System. Mol Cells. 2017;40(12):897-905.
24. Aguilera-Gomez A, Rabouille C. Membrane-bound organelles versus membrane-less compartments and their control of anabolic pathways in Drosophila. Dev Biol. 2017;428(2):310-317.
25. Lamb CA, Yoshimori T, Tooze SA. The autophagosome: origins unknown, biogenesis complex. Nat Rev Mol Cell Biol. 2013;14(12):759-74
26. Kovács GG, László L, Kovács J, Jensen PH, Lindersson E, Botond G, Molnár T, Perczel A, Hudecz F, Mezo G, Erdei A, Tirián L, Lehotzky A, Gelpi E, Budka H, Ovádi J. Natively unfolded tubulin polymerization promoting protein TPPP/p25 is a common marker of alpha-synucleinopathies. Neurobiol Dis. 2004;17(2):155-62.
27. Cianfrocco MA, DeSantis ME, Leschziner AE, Reck-Peterson SL. Mechanism and regulation of cytoplasmic dynein. Annu Rev Cell Dev Biol. 2015;31:83-108.
28. Reck-Peterson SL, Redwine WB, Vale RD, Carter AP. The cytoplasmic dynein transport machinery and its many cargoes. Nat Rev Mol Cell Biol. 2018;19(6):382-398.
29. Stavoe AKH, Holzbaur ELF. Axonal autophagy: Mini-review for autophagy in the CNS. Neurosci Lett. 2018. pii: S0304-3940(18)30194-0.
30. Yan J, Seibenhener ML, Calderilla-Barbosa L, Diaz-Meco MT, Moscat J, Jiang J, Wooten MW, Wooten MC. SQSTM1/p62 interacts with HDAC6 and regulates deacetylase activity. PLoS One. 2013;8(9):e76016.
31. Yan J. Interplay between HDAC6 and its interacting partners: essential roles in the aggresome-autophagy pathway and neurodegenerative diseases. DNA Cell Biol. 2014;33(9):567-80.
32. Calderilla-Barbosa L, Seibenhener ML, Du Y, Diaz-Meco MT, Moscat J, Yan J, Wooten MW, Wooten MC. Interaction of SQSTM1 with the motor protein dynein--SQSTM1 is required for normal dynein function and trafficking. J Cell Sci. 2014;127(Pt 18):4052-63.
33. Rapali P, Radnai L, Süveges D, Harmat V, Tölgyesi F, Wahlgren WY, Katona G, Nyitray L, Pál G. Directed evolution reveals the binding motif preference of the LC8/DYNLL hub protein and predicts large numbers of novel binders in the human proteome. PLoS One. 2011;6(4):e18818.
34. Rapali P, Szenes Á, Radnai L, Bakos A, Pál G, Nyitray L. DYNLL/LC8: a light chain subunit of the dynein motor complex and beyond. FEBS J. 2011;278(17):2980-96.

35. Rapali P, García-Mayoral MF, Martínez-Moreno M, Tárnok K, Schlett K, Albar JP, Bruix M, Nyitray L, Rodriguez-Crespo I. LC8 dynein light chain (DYNLL1) binds to the C-terminal domain of ATM-interacting protein (ATMIN/ASCIZ) and regulates its subcellular localization. Biochem Biophys Res Commun. 2011;414(3):493-8.
36. Barbar E. Dynein light chain LC8 is a dimerization hub essential in diverse protein networks. Biochemistry. 2008;47(2):503-8
37. King SM. Dynein-independent functions of DYNLL1/LC8: redox state sensing and transcriptional control. Sci Signal. 2008;1(47):pe51.
38. Lee KH, Lee S, Kim B, Chang S, Kim SW, Paick JS, Rhee K. Dazl can bind to dynein motor complex and may play a role in transport of specific mRNAs. EMBO J. 2006;25(18):4263-70.
39. Benison G, Karplus PA, Barbar E. Structure and dynamics of LC8 complexes with KXTQT-motif peptides: swallow and dynein intermediate chain compete for a common site. J Mol Biol. 2007;371(2):457-68.
40. Radnai L, Rapali P, Hódi Z, Süveges D, Molnár T, Kiss B, Bécsi B, Erdödi F, Buday L, Kardos J, Kovács M, Nyitray L. Affinity, avidity, and kinetics of target sequence binding to LC8 dynein light chain isoforms. J Biol Chem. 2010;285(49):38649-57.
41. Skultetyova L, Ustinova K, Kutil Z, Novakova Z, Pavlicek J, Mikesova J, Trapl D, Baranova P, Havlinova B, Hubalek M, Lansky Z, Barinka C. Human histone deacetylase 6 shows strong preference for tubulin dimers over assembled MTs. Sci Rep. 2017;7(1):11547.
42. Oláh J, Szénási T, Szunyogh S, Szabó A, Lehotzky A, Ovádi J. Further evidence for MT-independent dimerization of TPPP/p25. Sci Rep. 2017;7:40594.
43. Paik SR, Lee JH, Kim DH, Chang CS, Kim J. Aluminum-induced structural alterations of the precursor of the non-A beta component of Alzheimer's disease amyloid. Arch Biochem Biophys. 1997;344(2):325-34.
44. Na GC, Timasheff SN. Interaction of vinblastine with calf brain tubulin: multiple equilibria. Biochemistry. 1986;25(20):6214-22.
45. Bradford MM. A rapid and sensitive method for the quantitation of microgram quantities of protein utilizing the principle of protein-dye binding. Anal Biochem. 1976;72:248-54.
46. Szénási T, Oláh J, Szabó A, Szunyogh S, Láng A, Perczel A, Lehotzky A, Uversky VN, Ovádi J. Challenging drug target for Parkinson's disease: Pathological complex of the chameleon TPPP/p25 and alpha-synuclein proteins. Biochim Biophys Acta Mol Basis Dis. 2017;1863(1):310-323.

47. Höftberger R, Fink S, Aboul-Enein F, Botond G, Olah J, Berki T, Ovadi J, Lassmann H, Budka H, Kovacs GG. Tubulin polymerization promoting protein (TPPP/p25) as a marker for oligodendroglial changes in multiple sclerosis. Glia. 2010;58(15):1847-57.
48. Furumai R, Komatsu Y, Nishino N, Khochbin S, Yoshida M, Horinouchi S. Potent histone deacetylase inhibitors built from trichostatin A and cyclic tetrapeptide antibiotics including trapoxin. Proc Natl Acad Sci U S A. 2001;98(1):87-92.
49. Oláh J, Vincze O, Virók D, Simon D, Bozsó Z, Tõkési N, Horváth I, Hlavanda E, Kovács J, Magyar A, Szűcs M, Orosz F, Penke B, Ovádi J. Interactions of pathological hallmark proteins: tubulin polymerization promoting protein/p25, beta-amyloid, and alpha-synuclein. J Biol Chem. 2011;286(39):34088-100.
50. El-Agnaf OM, Salem SA, Paleologou KE, Curran MD, Gibson MJ, Court JA, Schlossmacher MG, Allsop D. Detection of oligomeric forms of alpha-synuclein protein in human plasma as a potential biomarker for Parkinson's disease. FASEB J. 2006;20(3):419-25.
51. Williams JC, Roulhac PL, Roy AG, Vallee RB, Fitzgerald MC, Hendrickson WA. Structural and thermodynamic characterization of a cytoplasmic dynein light chain-intermediate chain complex. Proc Natl Acad Sci U S A. 2007;104(24):10028-33.
52. Erdős G, Szaniszló T, Pajkos M, Hajdu-Soltész B, Kiss B, Pál G, Nyitray L, Dosztányi Z. Novel linear motif filtering protocol reveals the role of the LC8 dynein light chain in the Hippo pathway. PLoS Comput Biol. 2017;13(12):e1005885.
53. Tirián L, Hlavanda E, Oláh J, Horváth I, Orosz F, Szabó B, Kovács J, Szabad J, Ovádi J. TPPP/p25 promotes tubulin assemblies and blocks mitotic spindle formation. Proc Natl Acad Sci U S A. 2003;100(24):13976-81.
54. Kawaguchi Y, Kovacs JJ, McLaurin A, Vance JM, Ito A, Yao TP. The deacetylase HDAC6 regulates aggresome formation and cell viability in response to misfolded protein stress. Cell. 2003;115(6):727-38.
55. Pandey UB, Nie Z, Batlevi Y, McCray BA, Ritson GP, Nedelsky NB, Schwartz SL, DiProspero NA, Knight MA, Schuldiner O, Padmanabhan R, Hild M, Berry DL, Garza D, Hubbert CC, Yao TP, Baehrecke EH, Taylor JP. HDAC6 rescues neurodegeneration and provides an essential link between autophagy and the UPS. Nature. 2007;447(7146):859-63.
56. Liu Y, Peng L, Seto E, Huang S, Qiu Y. Modulation of histone deacetylase 6 (HDAC6) nuclear import and tubulin deacetylase activity through acetylation. J Biol Chem. 2012;287(34):29168-74.

57. Kreko-Pierce T, Eaton BA. The Drosophila LC8 homolog cut up specifies the axonal transport of proteasomes. J Cell Sci. 2017;130(19):3388-3398.
58. Singh PK, Roukounakis A, Weber A, Das KK, Sohm B, Villunger A, Garcia-Saez AJ, Häcker G. Dynein light chain binding determines complex formation and posttranslational stability of the Bcl-2 family members Bmf and Bim. Cell Death Differ. 2019 Jun 12. doi: 10.1038/s41418-019-0365-y. [Epub ahead of print]
59. Jespersen N, Estelle A, Waugh N, Davey NE, Blikstad C, Ammon YC, Akhmanova A, Ivarsson Y, Hendrix DA, Barbar E. Systematic identification of recognition motifs for the hub protein LC8. Life Sci Alliance. 2019 Jul 2;2(4). pii: e201900366. doi: 10.26508/lsa.201900366. Print 2019 Aug.
60. Asthana J, Kuchibhatla A, Jana SC, Ray K, Panda D. Dynein light chain 1 (LC8) association enhances microtubule stability and promotes microtubule bundling. J Biol Chem. 2012;287(48):40793-805.
61. Day CL, Puthalakath H, Skea G, Strasser A, Barsukov I, Lian LY, Huang DC, Hinds MG. Localization of dynein light chains 1 and 2 and their pro-apoptotic ligands. Biochem J. 2004;377(Pt 3):597-605.
62. den Hollander P, Kumar R. Dynein light chain 1 contributes to cell cycle progression by increasing cyclin-dependent kinase 2 activity in estrogen-stimulated cells. Cancer Res. 2006;66(11):5941-9.
63. Dorsett M, Schedl T. A role for dynein in the inhibition of germ cell proliferative fate. Mol Cell Biol. 2009;29(22):6128-39.
64. Yang CJ, Liu YP, Dai HY, Shiue YL, Tsai CJ, Huang MS, Yeh YT. Nuclear HDAC6 inhibits invasion by suppressing NF-κB/MMP2 and is inversely correlated with metastasis of non-small cell lung cancer. Oncotarget. 2015;6(30):30263-76.
65. Chen YM, Gerwin C, Sheng ZH. Dynein light chain LC8 regulates syntaphilin-mediated mitochondrial docking in axons. J Neurosci. 2009;29(30):9429-38.

11. FIGURE LEGENDS

Fig. 1. Multiple interactions of LC8-2 with TPPP/p25 and tubulin. (A) TPPP/p25 or tubulin was loaded to the LC8-2 affinity column as described in the Materials and Methods. The unbound (w1-w10) and bound (e1-e10) fractions were collected, and the amount of the given protein in each fraction was quantified by absorbance at 280 nm, the loaded amount of proteins was considered 100%. A representative experiment. (SDS-PAGE images of fractions are

presented in Supplementary Fig. 2). (B-D) Quantification of the interactions of LC8-2 with TPPP/p25 and/or tubulin by ELISA. (B) Saturation curves were obtained by addition of the FL (●), NT (Δ3–43) (○), CT (Δ175–219) (▲) and DT (Δ3–43/Δ175–219) (Δ) TPPP/p25 as well as α-synuclein (♦) to the LC8-2 isoform immobilized on the plate, and the binding was detected by specific TPPP/p25 or α-synuclein antibodies as described in the Materials and Methods. The binding constants (K_d) were evaluated from the saturation curves by non-linear curve fitting assuming single binding site hyperbola model. The data are presented as mean ± SD, n=3 for the various TPPP/forms, while n=2 for α-synuclein. (C-D) Tubulin at different concentrations alone (●) or pre-incubated with 100 nM TPPP/p25 (○) were added to the plate, then the binding of tubulin (C) and that of TPPP/p25 (D) were detected by specific tubulin and TPPP/p25 antibodies, respectively. Theoretical curves assuming exclusively binary (dashed line) or ternary (solid line) complexes are also shown. The data are presented as mean ± SD, n=3 for tubulin and tubulin preincubated with TPPP/p25, when the binding of tubulin was detected, and n=4 when the binding of TPPP/p25 was detected in the presence of tubulin.

Fig. 2. Structural consequences of the interaction of TPPP/p25 and LC8-2. (A-B) Secondary structural characteristics of TPPP/p25 and its complexes with tubulin (A) and LC8-2 (B) as detected by far-UV CD spectroscopy. (A) CD spectrum of TPPP/p25 (red line), tubulin (solid line), their mixture (dotted line), and the difference spectrum (dashed line) derived by the interaction-induced structural alteration. (B) The CD spectrum of TPPP/p25 (red line), LC8-2 (blue line), its complex with TPPP/p25 (dotted blue line), and their difference spectrum (dashed blue line) are shown. Difference ellipticities were calculated by subtracting the ellipticities of the individual proteins from that of their complex. Concentrations of the proteins: 7 μM LC8-2, 4 μM TPPP/p25 and 1 μM tubulin. (C) Effect of LC8-2 on the monomer-dimer equilibrium of TPPP/p25 as detected by sandwich ELISA. Monoclonal anti-TPPP/p25 antibody was immobilized on the plate, and 1 μM TPPP/p25 was added onto the plate pre-incubated without or with 0.5 μM LC8-2 or 2 μM LC8-2 or 100 μM DTE or 10 μM $ZnCl_2$. Then the same monoclonal TPPP/p25 antibody in biotinylated form was added and detected through peroxidase conjugated avidin reaction. The relative binding values are presented referring to the control (TPPP/p25 alone). The data are presented as mean ± SD, n=4 for control and DTE, n=3 for 0.5 μM LC8-2, 2 μM LC8-2 and $ZnCl_2$. *indicates the significant difference in the binding with respect to the control ($p<0.05$). (D) Effect of TPPP/p25 or DIC on the binding of FITC-BMF peptide to LC8-2 as determined by fluorescence polarization.

Fig. 3. Effect of LC8-2 on the TPPP/p25-induced tubulin polymerization. (A) Tubulin (6 μM) polymerization promoted by TPPP/p25 (3 μM) in the absence and presence of LC8-2 (10 μM). The tubulin polymerization was induced by the addition of TPPP/p25 or TPPP/p25 pre-incubated with LC8-2. LC8-2 (20 μM) alone added to tubulin is also shown. (B) Electron microscopic images of tubulin assemblies forming intact-like MT, bundled MT and aggregates induced by TPPP/p25 in the absence and presence of paclitaxel. Scale bar 100 nm. (Modified from [53]). (C-D) Pelleting experiments. TPPP/p25 (3 μM) and/or LC8-2 (10 μM) was added to tubulin (6 μM). Sample 1 and 5 as well as 4 and 6 are the same except the preincubation time (0 or 15 min) (C). (D) After centrifugation, the supernatant (S) and the pellet (P) fractions were loaded to SDS-PAGE. MM: molecular weight marker.

Fig. 4. HDAC6 as a new interacting partner of LC8-2. (A) HeLa extracts of control cells (lane 1) and cells transfected with 2 μg (lane 2) or 6 μg (lane 3) HDAC6 construct (cf. Material and Methods). Samples were prepared and analyzed by Western blot using polyclonal HDAC6 antibody; the loading control was tubulin. The images of Western blot indicate immunopositivities for HDAC6 and tubulin. Amido black dye was used to stain for total proteins on the Western blot membrane (see Supplementary Fig. 5). (B) The binding of HDAC6 from the extracts (1 mg/ml total protein) to the immobilized LC8-2 was quantified by specific HDAC6 antibody in an ELISA experiment. The data are presented as mean ± SD, n=4 for HeLa extract and HeLa cell extract with HDAC6 transfection (2), n=3 for HeLa cell extract with HDAC6 transfection (3). *Significant difference with respect to HeLa cell extract ($p<0.05$). (C) Then 100 nM TPPP/p25, 500 nM LC8-2 or their preincubated mixture were added to HDAC6 immobilized on the plate. The bindings of both TPPP/p25 and LC8-2 to HDAC6 were detected by specific antibodies. The values were normalized for a given protein alone. The data are presented as mean ± SD, n=6 for samples, when the binding of TPPP/p25 was detected, n=5 when the binding of LC8-2 was detected. *Significant difference with respect to the given protein alone versus their mixture ($p<0.05$).

Fig. 5. Effect of LC8-2 on the tubulin deacetylase activity of HDAC6. (A) HDAC6-transfected HeLa cell extracts were incubated with tubulin with or without LC8-2 (10 μM) or TSA (1 μM), then subjected to Western blot. The blot was developed using a monoclonal mouse antibody against acetylated α-tubulin at Lys-40, antibody binding was revealed by anti-mouse

IgG-peroxidase conjugate. The values were normalized with respect to that measured for tubulin alone. The data are presented as mean ± SD, n=7 for tubulin and tubulin + extract + TSA, n=5 for extract, tubulin + extract and tubulin + extract + LC8-2. *Significant difference with respect to tubulin alone ($p<0.05$). The images of a full-length representative Western blot (developed using acetyl-tubulin antibody, then amido black solution) are presented in Supplementary Fig. 6. (B) Acetyl-tubulin levels in HeLa cells transfected with TPPP/p25, LC8-2 or both proteins are shown. Acetyl-tubulin signals were analyzed by immunofluorescence microscopy as described in the Materials and Methods, in each case at least 50 cells were analyzed. *Significant difference with respect to control cells, and TPPP/p25 transfected cells versus TPPP/p25 + LC8-2 ones ($p<0.05$).

Fig. 6. Visualization of the interactions of LC8-2 with TPPP/p25 and HDAC6 in living HeLa cells as detected by BiFC technology coupled with immunofluorescence microscopy. (A) Scheme of the applied BiFC constructs. (B) Representative images of EGFP-HDAC6 and mCherry-LC8-2 localization in HeLa cells. The intrinsic fluorescence of the labeled proteins were measured (EGFP as green and mCherry as red); nuclei were counterstained with DAPI (blue). Note that HDAC6 localizes mainly in the cytosol, while LC8-2 can be found homogeneously in both the cytosol and the nucleus. Scale bar: 10 μm. (C) The LC8-2-TPPP/p25 complex (green) co-localizes with the MT network (red), while the complex of LC8-2-HDAC6 distributed homogenously in the cytosol and translocated into the nucleus as well. The MT network was stained with Alexa546, nuclei were counterstained with DAPI (blue). Scale bar: 10 μm. (D) The effect of unlabeled TPPP/p25 or HDAC6 as competitors on the BiFC signals of LC8-2-TPPP/p25 or LC8-2-HDAC6, respectively, was quantified as described in the Materials and Methods. The data are presented as mean ± SD, in each case at least 40 cells were analyzed. *Significant difference with respect to the BiFC complex alone ($p<0.05$). (E) The co-localization of LC8-2-HDAC6 BiFC complex (green) and TPPP/p25 (red) and the translocation of the BiFC complex into the nucleus. Nuclei were counterstained with DAPI (blue). Scale bar: 10 μm.

Fig. 7. Binary and ternary complexes of the MT regulatory proteins. The apparent dissociation constants of the binary complexes determined with recombinant proteins are K_d = 12.0 ± 3 nM for LC8-2 and TPPP/p25, K_d = 1740 ± 420 nM for LC8-2 and tubulin, K_d = 10.5 ± 1.2 nM for TPPP/p25 and tubulin [49], K_d = 5.3 ± 0.8 nM for TPPP/p25 and HDAC6 [16], and K_d = 9900 ± 2200 nM for tubulin and HDAC6 [16], respectively. Ternary complexes are DYNLL/LC8-TPPP/p25-tubulin/MT (green/yellow) and DYNLL/LC8-TPPP/p25-HDAC6 (red/yellow); DYNLL/LC8 and TPPP/p25 are involved in both ternary complexes.

Fig. 8: Tentative model of the binding of the toxic aggregates of the misfolded proteins formed at abnormal or pathological conditions to the cargo-HDAC6-dynein motor complex by the involvement of DYNLL/LC8-TPPP/p25 complex in order to be transported to the aggresome on the acetylated MT network.

Figure 1

Click here to download high resolution image

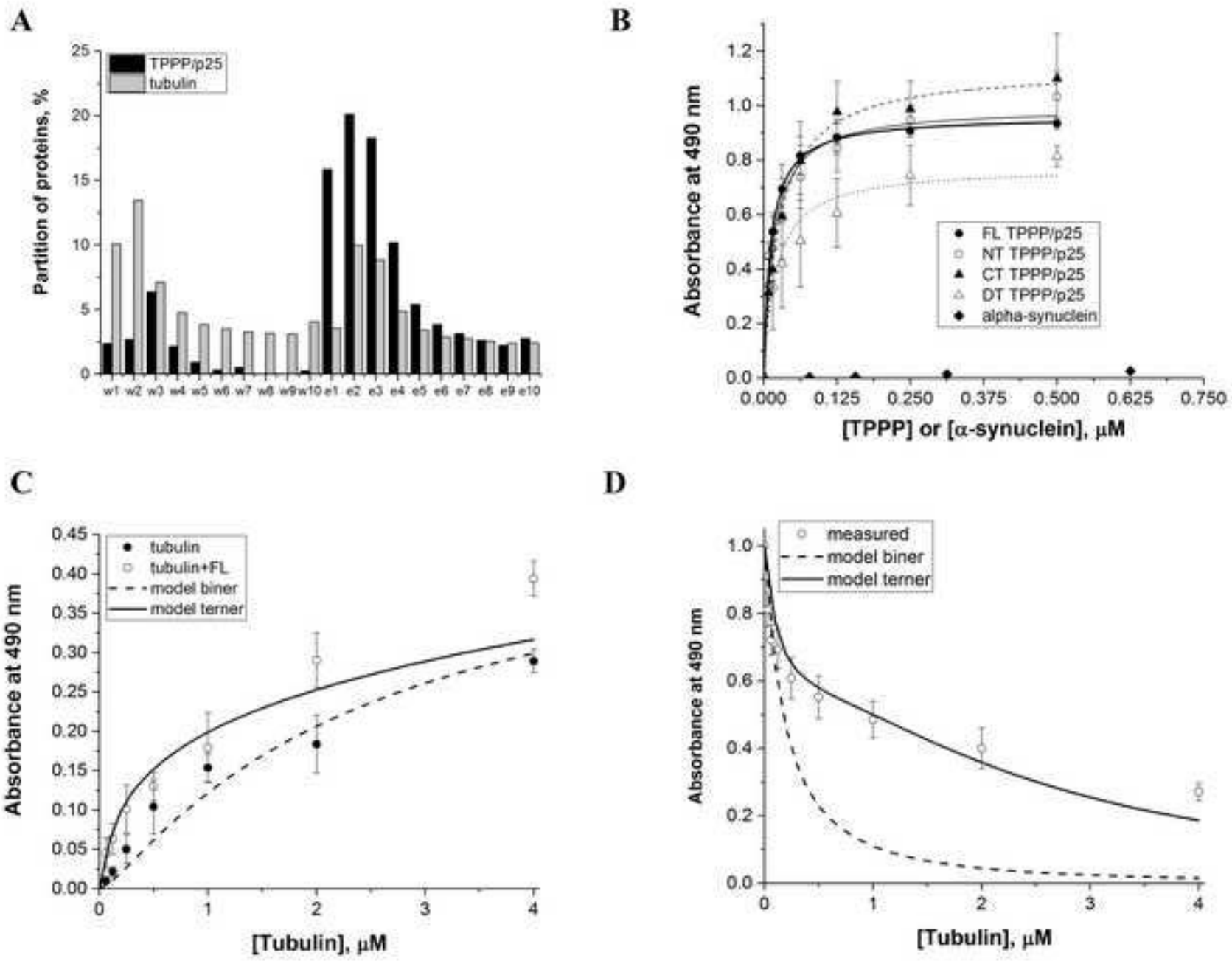

Figure 2

Click here to download high resolution image

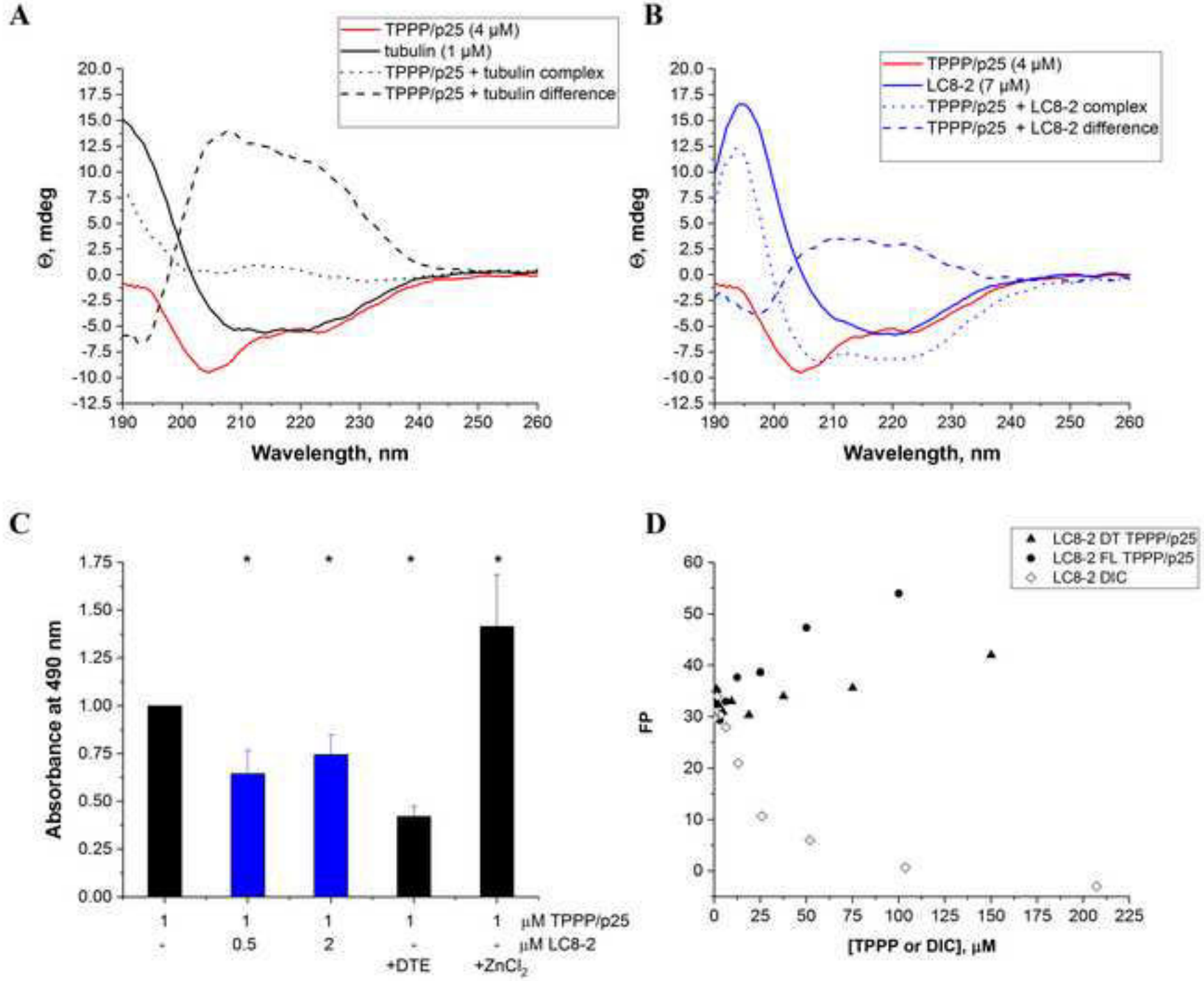

Figure 3

Click here to download high resolution image

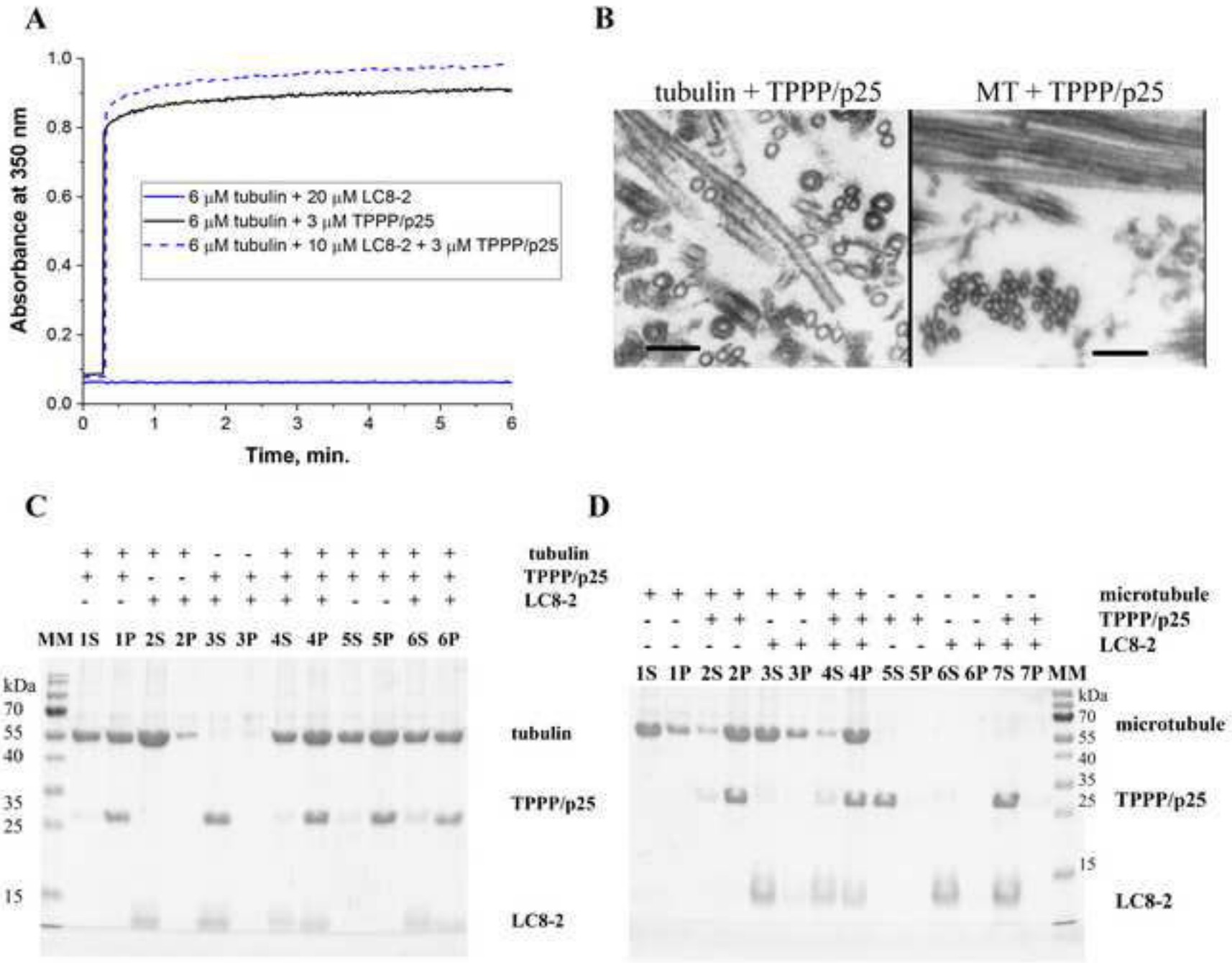

Figure 4

Click here to download high resolution image

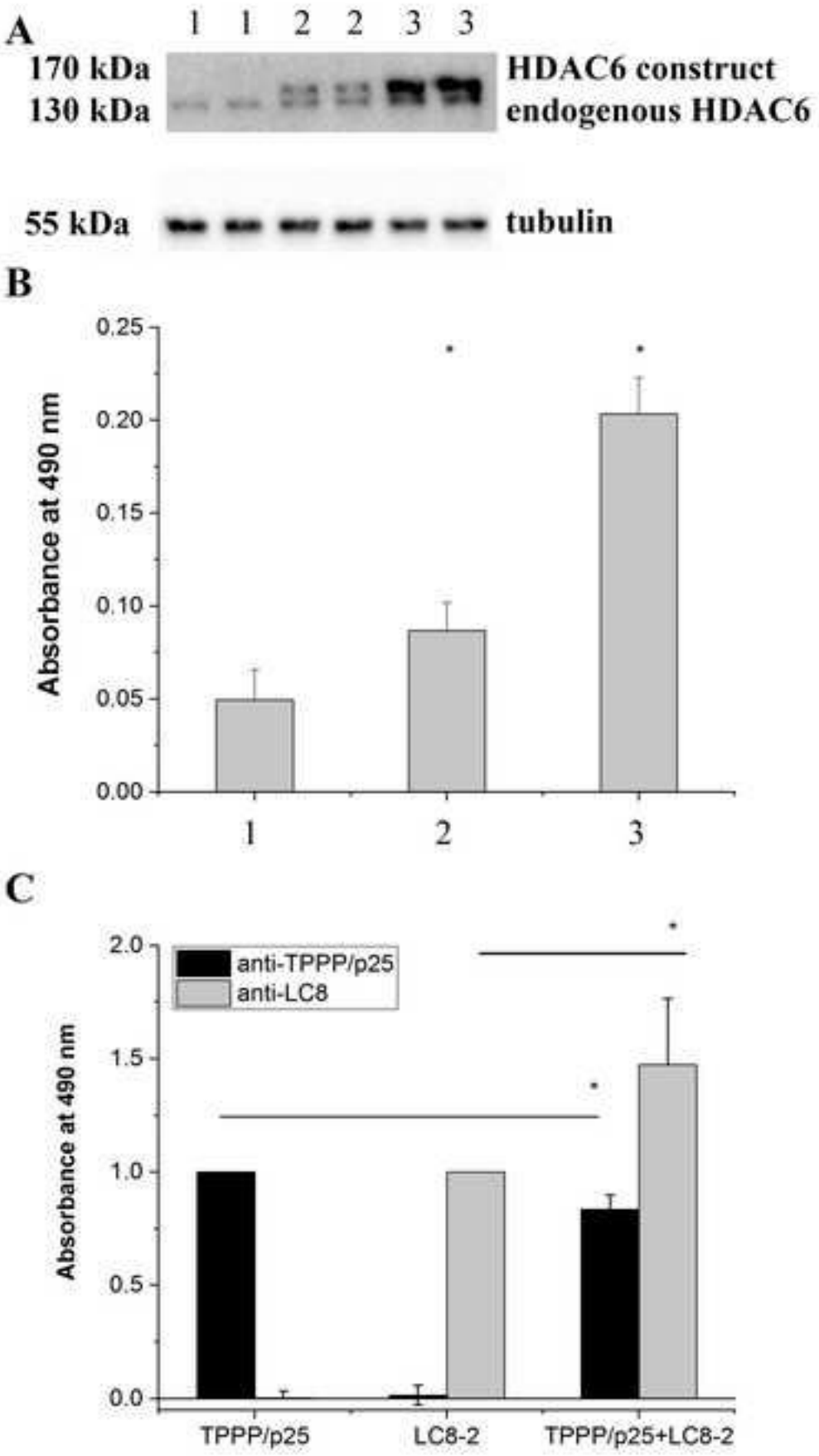

Figure 5

Click here to download high resolution image

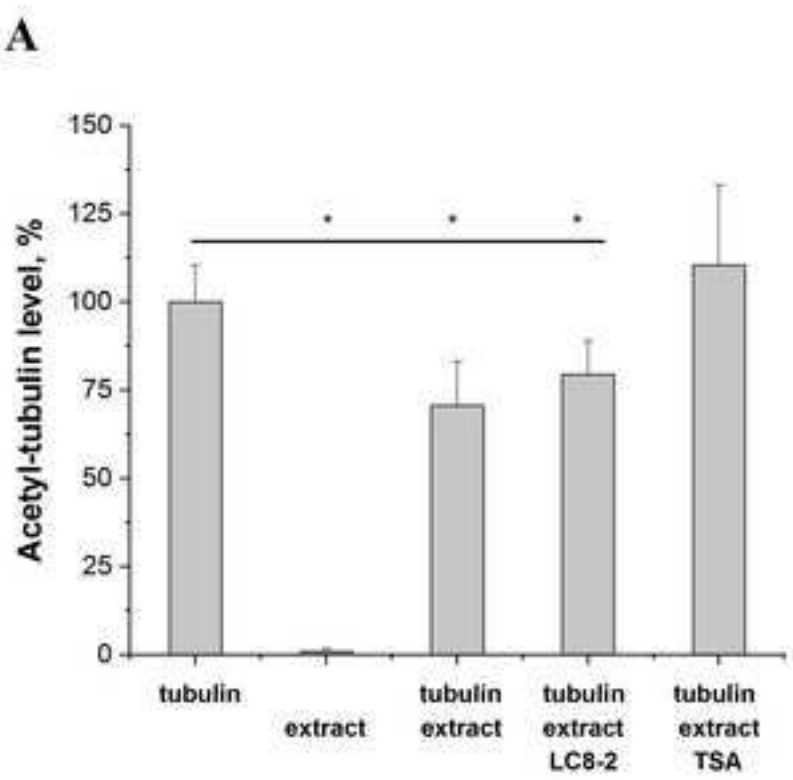

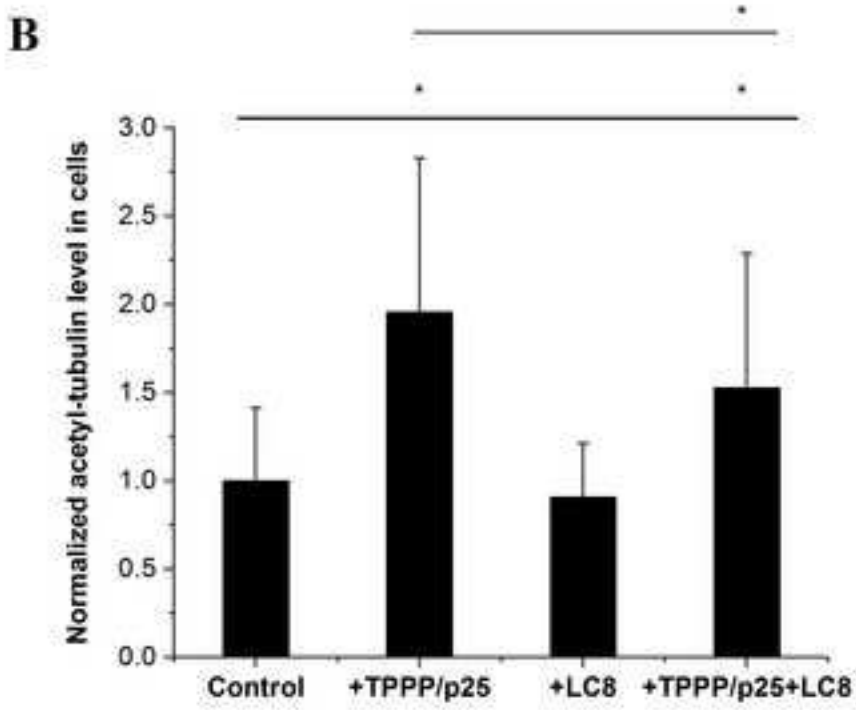

Figure 6

Click here to download high resolution image

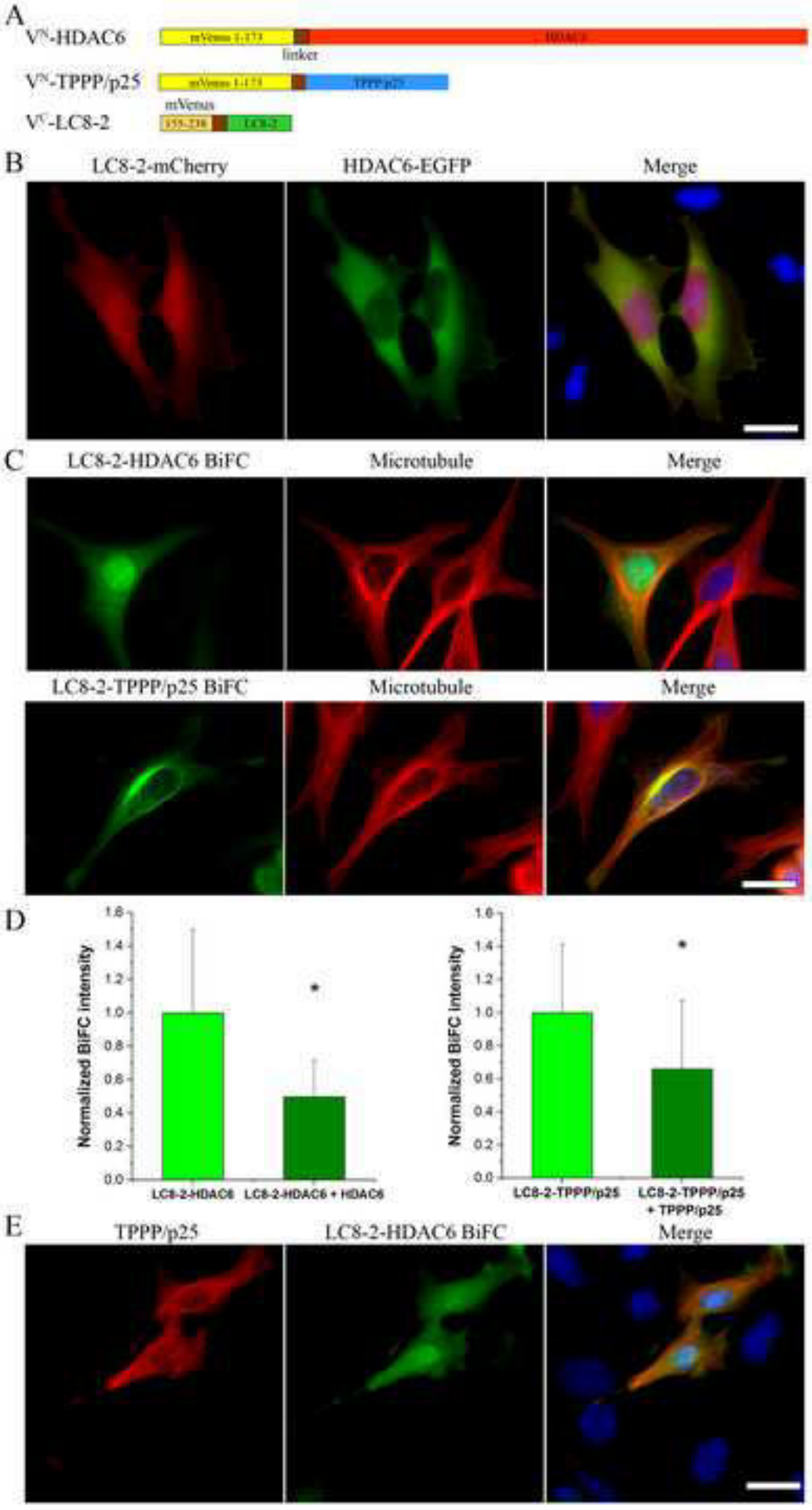

Figure 7
Click here to download high resolution image

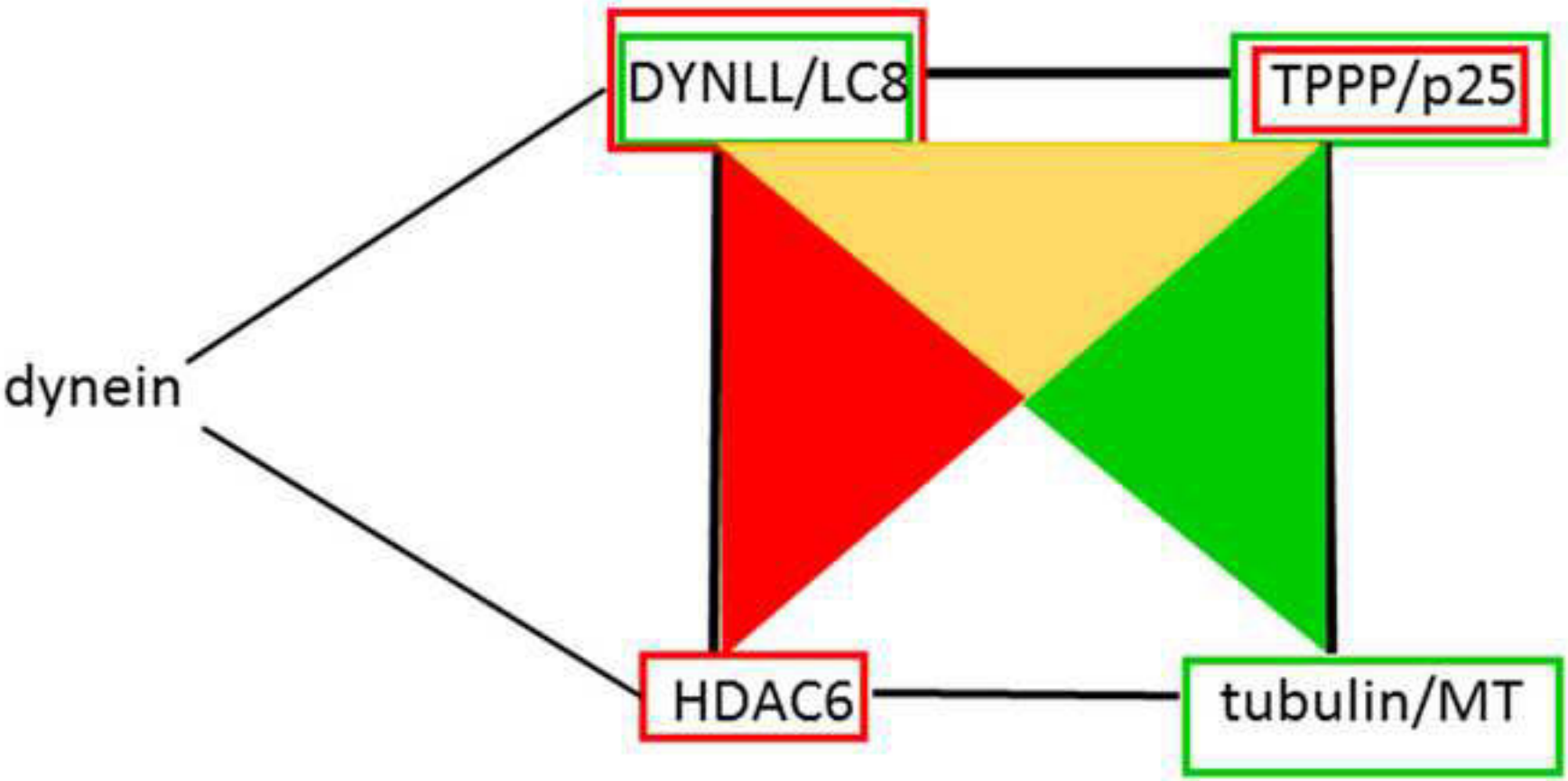

Figure 8

Click here to download high resolution image

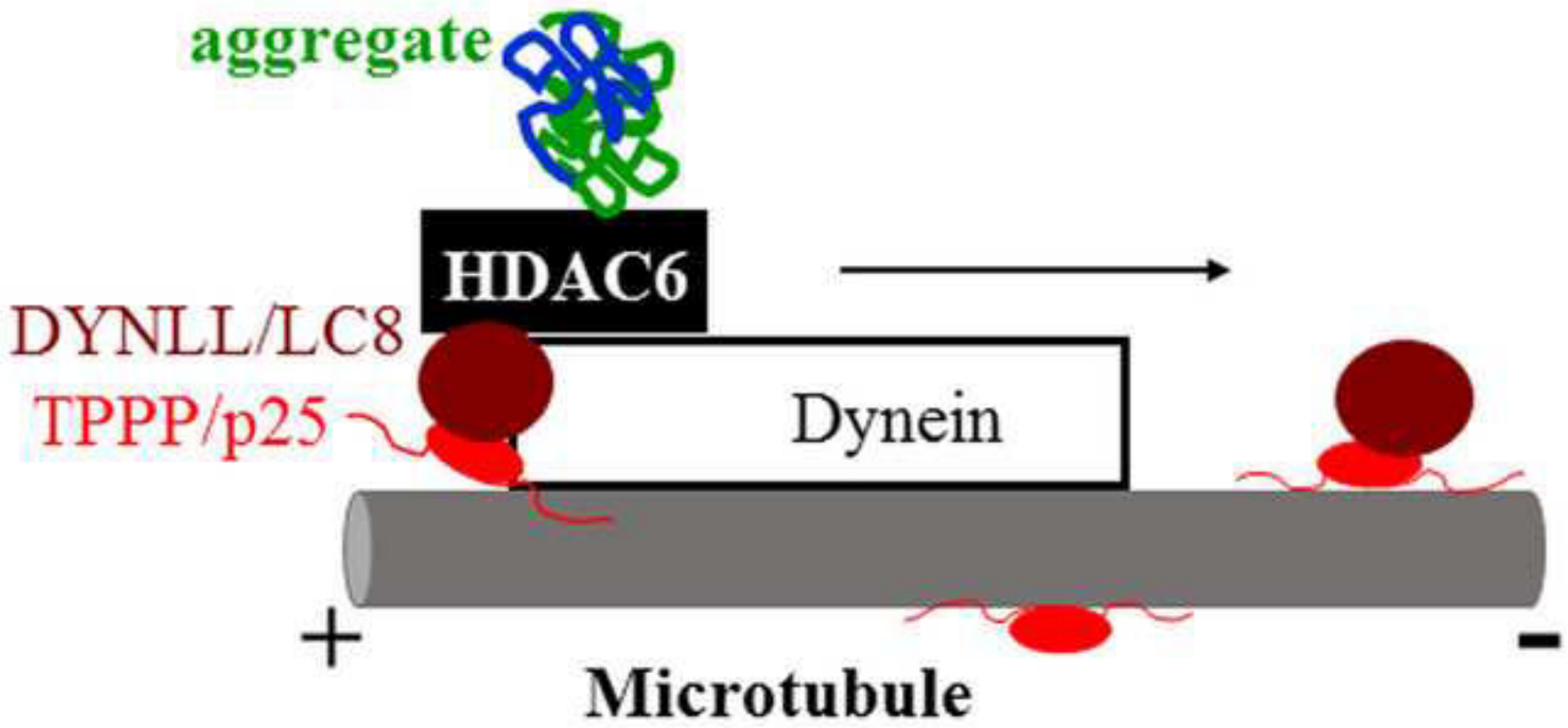

INTERACTIONS BETWEEN TWO REGULATORY PROTEINS OF MICROTUBULE DYNAMICS, HDAC6, TPPP/p25, AND THE HUB PROTEIN, DYNLL/LC8

SUPPLEMENTARY MATERIAL

Supplementary materials and methods

Plasmid constructs

pBiFC-V^{N1-173}-SYN was prepared and purified as described previously [1].

Cell culture, manipulation and images

Sample preparation and image aquisition of the empty Venus (V^C and V^N) and V^C-LC8-2 and V^N-SYN BiFC were the same as described in the Materials and methods section.

Confocal microscopy

The confocal microscopic images of transfected HeLa cells were acquired with a Zeiss LSCM 710 microscope using an oiled 40× NA = 1.4 Plan Apo objective. Nuclei were stained by 0.5 µg/mL Hoechst 33342 for 5 minutes during the last wash in immunochemistry preparation. Analysis of co-localization was measured using the line-profile tool in Zeiss Zen 2010 SP1 program on 1.0 µm slice of expressing cells.

Supplementary Reference

1. Szénási T, Oláh J, Szabó A, Szunyogh S, Láng A, Perczel A, Lehotzky A, Uversky VN, Ovádi J. Challenging drug target for Parkinson's disease: Pathological complex of the chameleon TPPP/p25 and alpha-synuclein proteins. Biochim Biophys Acta Mol Basis Dis. 2017;1863(1):310-323.
2. Tőkési N, Oláh J, Hlavanda E, Szunyogh S, Szabó A, Babos F, Magyar A, Lehotzky A, Vass E, Ovádi J. Identification of motives mediating alternative functions of the neomorphic moonlighting TPPP/p25. Biochim Biophys Acta. 2014;1842(4):547-57.

Mathematical model

Equations and definitions for the mathematical model

Dissociation constants:

K_1 = [TPPP/p25][tubulin]/[TPPP/p25-tubulin]

K_2 = [TPPP/p25][LC8]/[TPPP/p25-LC8]

K_3 = [LC8][tubulin]/[LC8-tubulin]

K_4 = [TPPP/p25-LC8]/[TPPP/p25-LC8-tubulin]

Time dependence of the concentration of the different species:

$d[TPPP/p25]/dt = -k_{1f}[TPPP/p25][tubulin] + k_{1r}[TPPP/p25\text{-}tubulin] - k_{2f}[TPPP/p25][LC8] + k_{2r}[TPPP/p25\text{-}LC8]$

$d[tubulin]/dt = -k_{1f}[TPPP/p25][tubulin] + k_{1r}[TPPP/p25\text{-}tubulin] - k_{3f}[tubulin][LC8] + k_{3r}[tubulin\text{-}LC8] - k_{4f}[tubulin][TPPP/p25\text{-}LC8] + k_{4r}[TPPP/p25\text{-}LC8\text{-}tubulin]$

$d[LC8]/dt = -k_{2f}[TPPP/p25][LC8] + k_{2r}[TPPP/p25\text{-}LC8] - k_{3f}[tubulin][LC8] + k_{3r}[tubulin\text{-}LC8]$

$d[TPPP/p25\text{-}tubulin]/dt = k_{1f}[TPPP/p25][tubulin] - k_{1r}[TPPP/p25\text{-}tubulin]$

$d[TPPP/p25\text{-}LC8]/dt = -k_{2f}[TPPP/p25][LC8] + k_{2r}[TPPP/p25\text{-}LC8] - k_{4f}[tubulin][TPPP/p25\text{-}LC8] + k_{4r}[TPPP/p25\text{-}LC8\text{-}tubulin]$

$d[tubulin\text{-}LC8]/dt = k_{3f}[tubulin][LC8] - k_{3r}[tubulin\text{-}LC8]$

$d[TPPP/p25\text{-}LC8\text{-}tubulin]/dt = k_{4f}[tubulin][TPPP/p25\text{-}LC8] - k_{4r}[TPPP/p25\text{-}LC8\text{-}tubulin]$

Mass conservation equation

$[TPPP/p25]_{total} = [TPPP/p25] + [TPPP/p25\text{-}tubulin] + [TPPP/p25\text{-}LC8] + [TPPP/p25\text{-}LC8\text{-}tubulin]$

$[LC8]_{total} = [LC8] + [tubulin\text{-}LC8] + [TPPP/p25\text{-}LC8] + [TPPP/p25\text{-}LC8\text{-}tubulin]$

$[tubulin]_{total} = [tubulin] + [TPPP/p25\text{-}tubulin] + [tubulin\text{-}LC8] + [TPPP/p25\text{-}LC8\text{-}tubulin]$

Supplementary Table S1. Parameters used for modelling.

Parameter		Value	Unit
total concentration of TPPP/p25	$[TPPP/p25]_{total}$	0.1	μM
total concentration of tubulin	$[tubulin]_{total}$	0-4.0	μM
total concentration of LC8	$[LC8]_{total}$	0.2	μM
dissociation constant of TPPP/p25 with tubulin[#]	$K_1 = k_{1r}/k_{1f}$	0.010	μM
dissociation constant of TPPP/p25 with LC8[#]	$K_2 = k_{2r}/k_{2f}$	0.015	μM
dissociation constant of tubulin with LC8[#]	$K_3 = k_{3r}/k_{3f}$	2.5	μM
dissociation constant of tubulin with TPPP/p25-LC8[*]	$K_4 = k_{4r}/k_{4f}$	0/0.10	μM

[#] Experimental values are based on the ELISA experiments (see Fig. 1). *0 μM for the binary and 0.10 μM for the ternary model. The rate constants for the evaluation of the model are derived from the K_d values by taking the k_f values to be 1.

Supplementary Figures

Supplementary Fig. 1

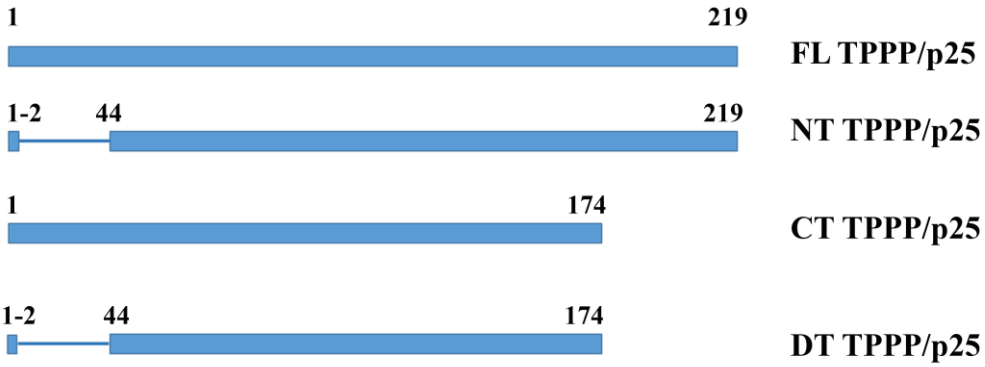

Scheme of the human recombinant FL TPPP/p25 and the various truncated forms. N-terminal truncated TPPP/p25 (NT, Δ3–43), C-terminal truncated TPPP/p25 (CT, Δ175–219) and double truncated TPPP/p25 (DT, Δ3–43/Δ175–219) [2].

Supplementary Fig. 2

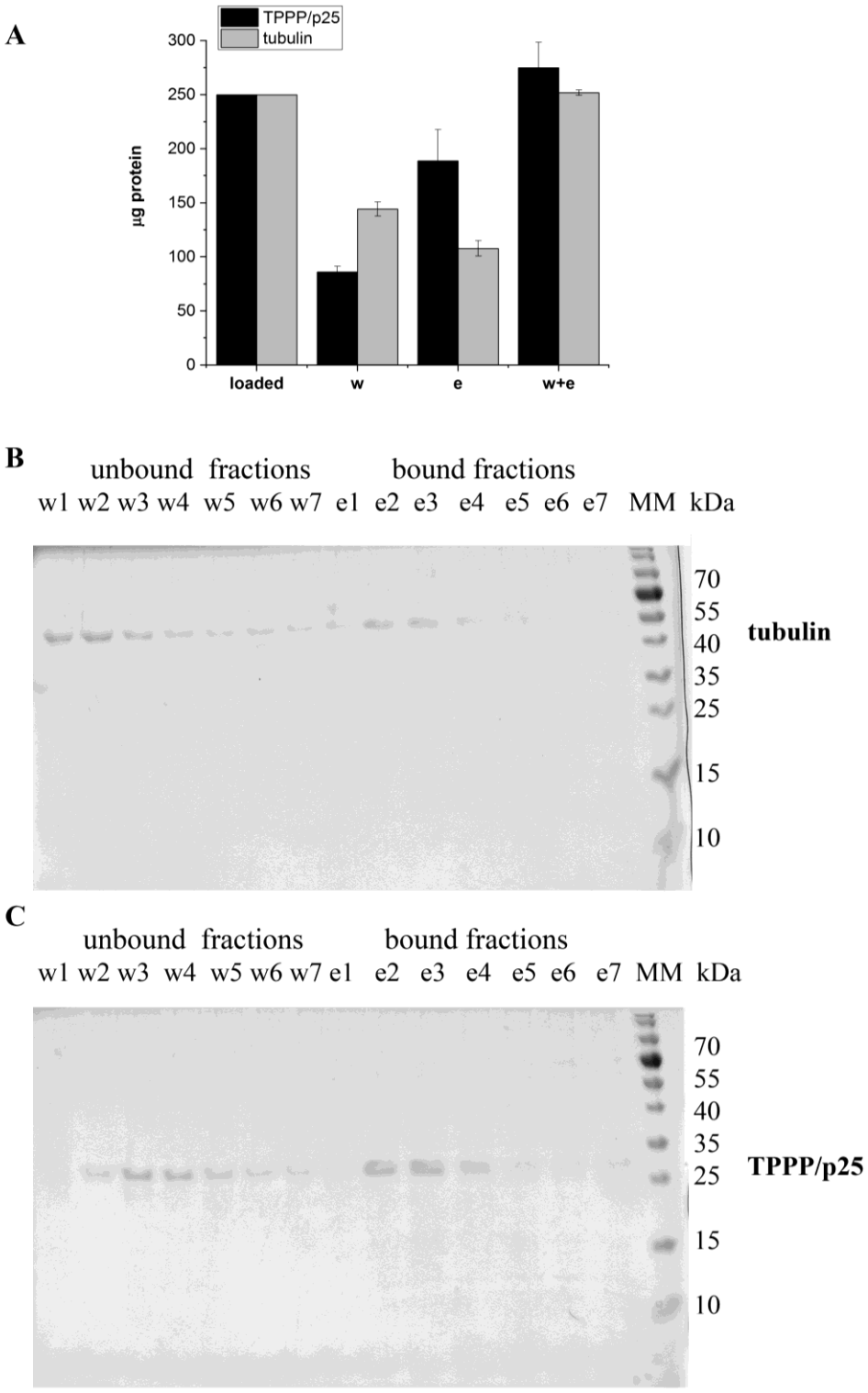

Interaction of LC8-2 with TPPP/p25 or tubulin. TPPP/p25 (250 µg) or tubulin (250 µg) was loaded to the LC8-2 affinity column as described in the Materials and Methods. (A) The unbound (w1-w10) and bound (e1-e10) fractions were collected, and the amount of the given protein in each fraction was quantified by absorbance at 280 nm. The amount of tubulin and TPPP/p25 in the unbound and bound fractions were analyzed by SDS-PAGE as well. (B-C) Representative SDS-PAGE images of tubulin (B) and TPPP/p25 (C).

Supplementary Fig. 3

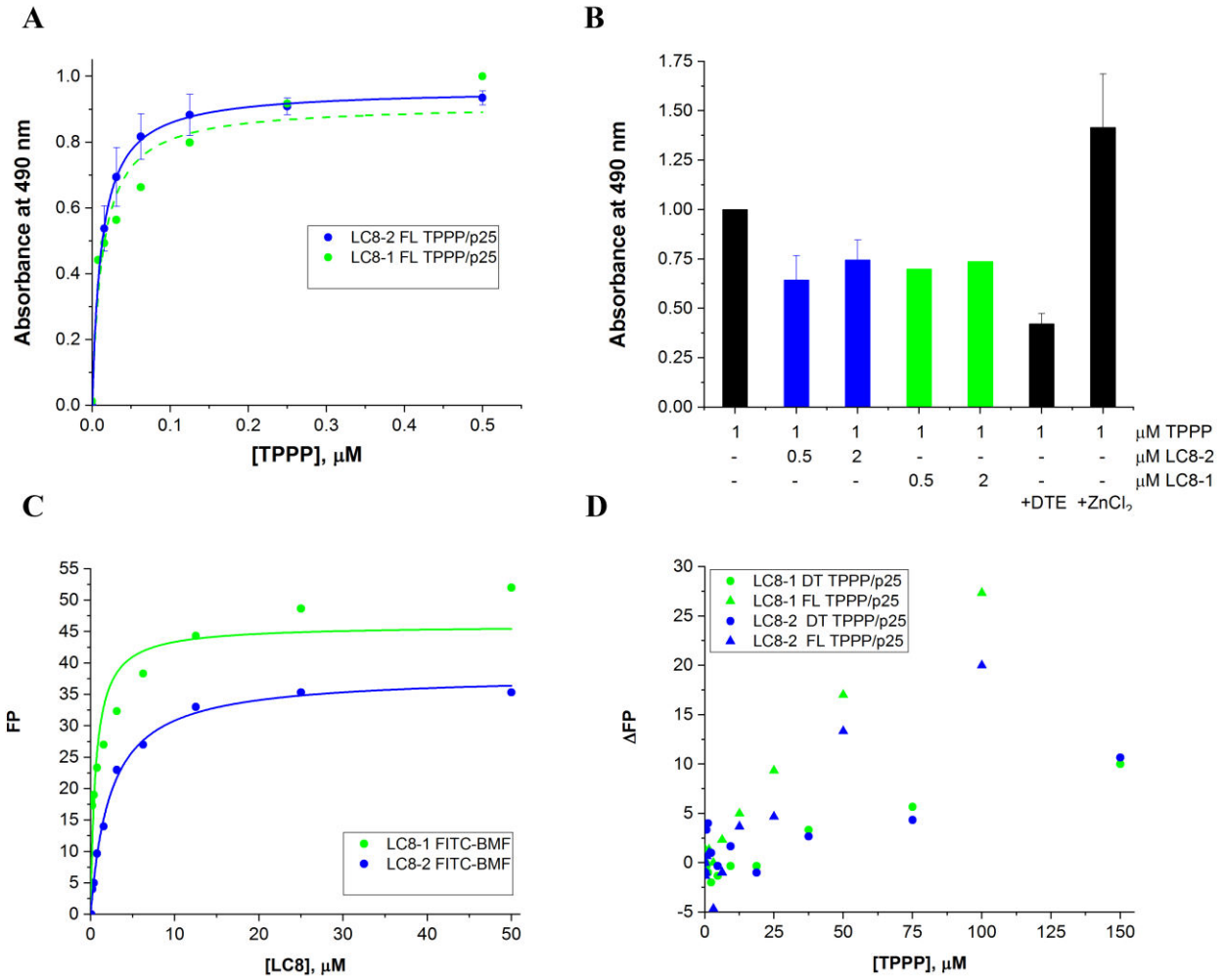

Multiple interactions of LC8-1 with TPPP/p25 and tubulin. (A) Quantification of the interactions of LC8-1 and LC8-2 with TPPP/p25 by ELISA. Saturation curves of TPPP/p25, when the plate was coated with the LC8-1 and LC8-2 isoforms. (B) Effect of LC8-1 and LC8-2 on the monomer-dimer equilibrium of TPPP/p25 as detected by sandwich ELISA. Monoclonal TPPP/p25 antibody was immobilized on the plate, and 1 μM TPPP/p25 was added onto the plate pre-incubated without or with 0.5 μM or 2 μM LC8 isoforms or 100 μM DTE or 10 μM $ZnCl_2$. Then the same monoclonal TPPP/p25 antibody was added in biotinylated form, which was detected through peroxidase conjugated avidin reaction. The values were normalized with respect to that measured for TPPP/p25 alone. (C) FP assay. Direct titration of the FITC-BMF peptide (50 nM) with LC8 isoforms. (D) Effect of TPPP/p25 forms on the binding of FITC-BMF peptide to LC8-1 or LC8-2 as determined by FP. Difference FP is shown.

Supplementary Fig. 4

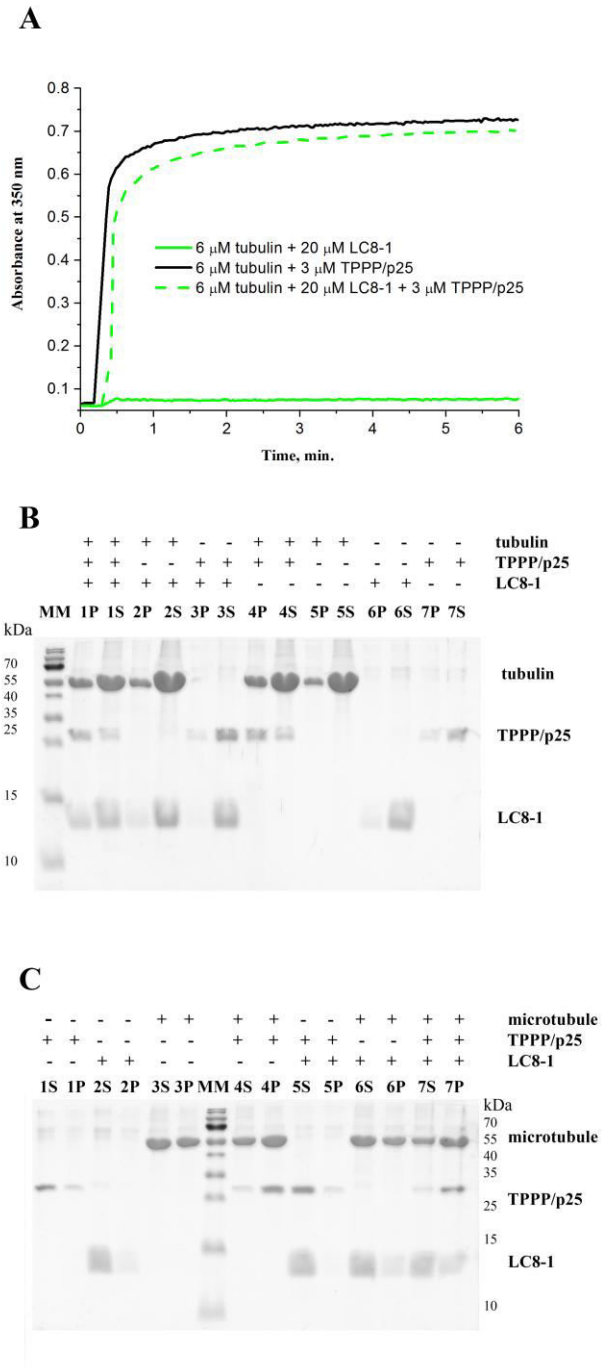

Effect of LC8-1 on the TPPP/p25-induced tubulin polymerization. (A) Tubulin (6 μM) polymerization promoted by TPPP/p25 (3 μM) in the absence and presence of LC8-1 (20 μM). The tubulin polymerization was induced by the addition of TPPP/p25 or TPPP/p25 pre-incubated with LC8-1. LC8-1 (20 μM) alone added to tubulin is also shown. (B-C) Pelleting experiments. TPPP/p25 (3 μM) and/or LC8-1 (10 μM) was incubated with tubulin (6 μM) or paclitaxel-assembled MTs. After centrifugation, the supernatant (S) and the pellet (P) fractions were loaded to SDS-PAGE.

Supplementary Fig. 5

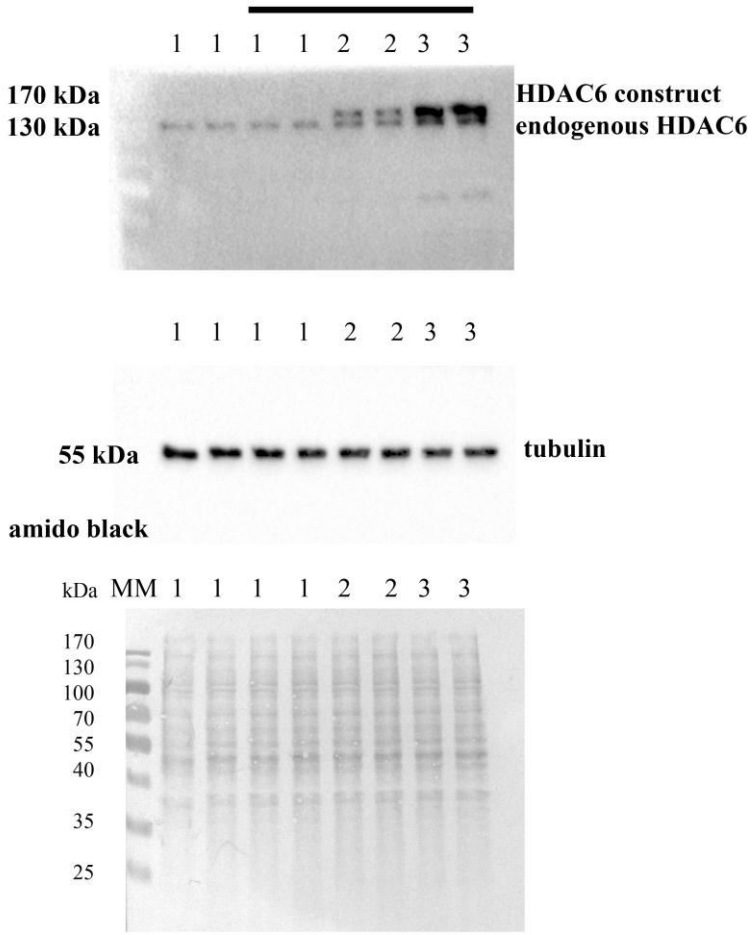

Western blot of HeLa extracts. HeLa extracts of control cells (lane 1) and cells transfected with 2 µg (lane 2) or 6 µg (lane 3) HDAC6 construct (cf. Material and Methods). Samples were prepared and analyzed by Western blot using polyclonal HDAC6 antibody; the loading control was tubulin. The images of a representative Western blot (developed using tubulin and HDAC6 antibodies, then amido black solution) are presented. The lanes indicated by a black line are presented in Fig. 4A.

Supplementary Fig. 6

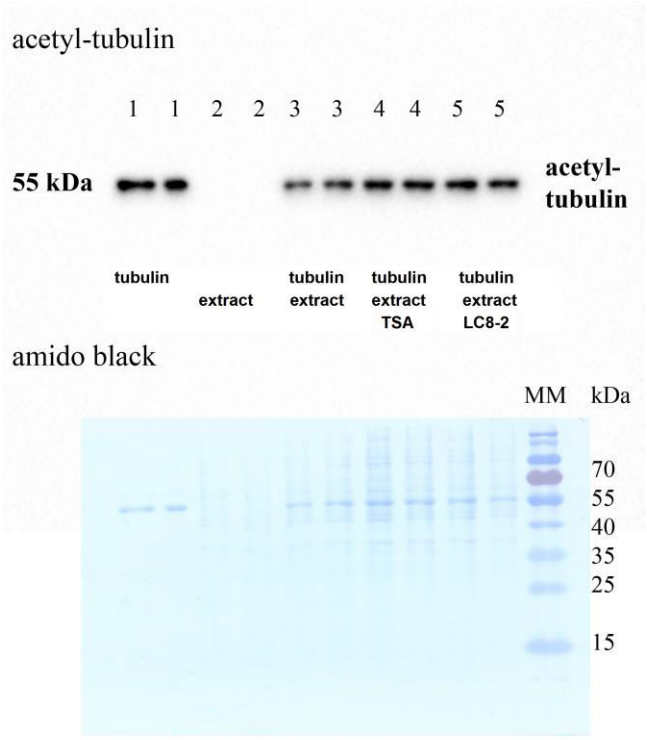

Effect of LC8-2 on the tubulin deacetylase activity of HDAC6. HDAC6-transfected HeLa cell extracts were incubated with tubulin with or without LC8-2 (10 μM) or TSA (1 μM), then subjected to Western blot. The blot was developed using a monoclonal mouse antibody against acetylated α-tubulin at Lys-40, antibody binding was revealed by anti-mouse IgG-peroxidase conjugate. The images of a full-length representative Western blot (developed using acetyl-tubulin antibody, then amido black solution) are presented.

Supplementary Fig. 7

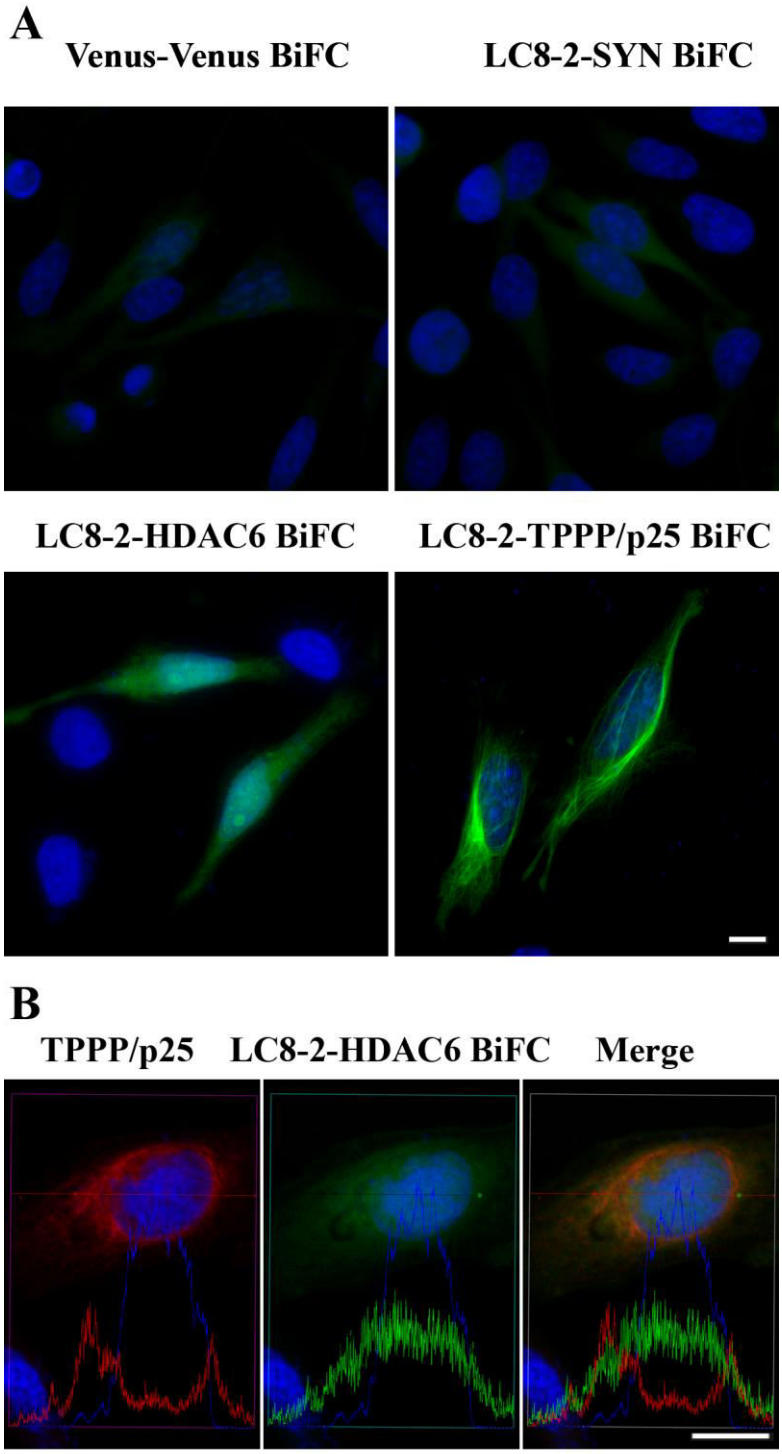

Visualization of the interactions of LC8-2 with TPPP/p25 and HDAC6 in living HeLa cells as detected by immunofluorescence microscopy coupled with BiFC technology. (A) Representative BiFC images with appropriate negative controls. The minimal emissions of the empty V^C-V^N and the LC8-2-SYN BiFC plasmid pairs are presented, in contrast to the LC8-2-HDAC6 or LC8-2-TPPP/p25 signals. Nuclei were counterstained with DAPI (blue). Scale bar: 10 μm. (B) Line-scan analysis of TPPP/p25 (red), V^C-LC8-2-V^N-HDAC6 (green) and the nucleus by confocal microscopy. TPPP/p25 seemed to be aligned along the thicker, likely bundled MT network in the transiently transfected HeLa cell, while the LC8-2-HDAC6 complex (green) distributed both in the cytosol and the nucleus. Note the strong presence of the BiFC complex in the nucleus where TPPP/p25 is absent. In the cytosol, there are areas with variable co-localization of TPPP/p25 with the BiFC complex, which remained predominantly diffuse. Nuclei were counterstained with DAPI (blue). Scale bar: 10 μm.